



ELSEVIER

Available online at www.sciencedirect.com**ScienceDirect**

Acta Materialia 94 (2015) 224–243

www.elsevier.com/locate/actamat

Microstructure and transformation texture evolution during α precipitation in polycrystalline α/β titanium alloys – A simulation study

R. Shi, N. Zhou,¹ S.R. Niezgoda and Y. Wang**Department of Materials Science and Engineering, The Ohio State University, 2041 College Road, Columbus, OH 43210, USA*

Received 5 March 2015; revised 12 March 2015; accepted 21 April 2015

Available online 21 May 2015

Abstract—A three-dimensional phase field model of $\beta \rightarrow \alpha$ transformation in polycrystalline Ti–6Al–4V (wt.%) alloys is formulated and used to study variant selection and microstructure evolution under different processing conditions and starting β phase textures. Degrees of variant selection at both individual β grain and polycrystalline β volume element levels and their connections to the final micro- and macro-texture of α precipitates are analyzed and correlated with the processing parameters. It is found that local stresses in an elastically anisotropic and inhomogeneous polycrystalline volume element lead to obvious variant selection. Under certain pre-strains, a local volume element of a polycrystalline β sample considered in the simulations could end up with a relatively weak micro- and macro-texture of the transformed α phase if it has a strong starting β phase texture. Moreover, a Fix-End (clamped) boundary constraint to the volume element is found to be more favorable than a Free-End (relaxed) one in preventing the formation of strong transformation texture irrespective of the strength of the starting β phase texture. Other factors contributing to variant selection and transformation texture development are also discussed. The results could shed light on how to control processing conditions and internal stresses to reduce transformation texture at both the individual β grain and the polycrystalline volume element level.

© 2015 Acta Materialia Inc. Published by Elsevier Ltd. All rights reserved.

Keywords: Variant selection; Phase transformation; Micro-texture; Ti–6Al–4V; Phase-field modeling

1. Introduction

Exploiting solid–solid phase transformation during thermo-mechanical processing is one of the most effective and efficient means to produce desired microstructures for many technically important materials including steels [1], light metals (e.g. Titanium, Magnesium and Aluminum alloys) [2] and shape memory alloys [3], to name a few. Often well-defined orientation relationships (ORs) exist between the parent and transformed product phases. Examples include, but are not limited to, Kurdjumov and Sachs [4] (K–S) and Nishiyama and Wassermann [5,6] (N–W) ORs in steels when austenite (fcc) transforms to martensite (bcc or bct) following the Bain lattice correspondence [7] (LC); Burgers [8] and Pitsch [9] ORs in titanium and zirconium alloys when the high-temperature β (bcc) phase transforms to the low temperature α (hcp) phase following the Burgers LC. As a consequence, if the parent phase grains have preferred crystallographic orientations or a crystallographic texture, this parent texture will be passed onto or constrain the texture of the transformed state. This is often referred to as texture transformation

and the resulting is termed the “transformation texture”. If symmetry breaking accompanies the phase transformation such as the examples mentioned above, there will be multiple orientation variants (OVs) of the product phase corresponding to a given parent phase grain. For example, during the β ($Im\bar{3}m$) to α ($P6_3mmc$) transformation in titanium alloys, there are 12 possible orientation variants of the α phase for a given β orientation which satisfies the Burgers orientation relationship (BOR), $\{0001\}_\alpha || \{011\}_\beta, \langle 11\bar{2}0 \rangle_\alpha || \langle 111 \rangle_\beta$.

The statistical and spatial distributions of OVs of a product phase define the transformation texture, which plays an important role in determining the properties and service performance of the alloys. In Ti alloys, for example, the texture of the highly anisotropic hcp α phase exhibits a strong influence on the elastic and plastic properties. In addition, the character of α/β interfaces and their spatial distribution are equally important microstructural features that determine the deformation mechanisms and mechanical behavior of the alloys [10,11]. If all the 12 OVs have more or less equal population or volume fraction in a β grain, then the transformation texture is randomized, which is extremely beneficial to the fatigue properties of the alloys. However, a completely random α texture is almost impossible to achieve because preferential variant selection (VS) occurs frequently in response to microstructural, temperature and stress fields, spanning several length scales

* Corresponding author. Tel.: +1 614 292 0682; e-mail: wang363@osu.edu

¹ Permanent address: GE Global Research, 1 Research Circle, Niskayuna, NY 12309, USA.

from subgrain structure to the polycrystalline β aggregate, experienced during heat treatment alone and thermal-mechanical processing (TMP) [12], the latter being a combination of working and heat treatment. In some alloys such as Ti–6Al–4V (in wt.%), uncontrolled VS could lead to the formation of large regions of the α phase with a common crystallographic feature (such as common basal $(0001)_\alpha$ pole, or common orientation), i.e., “macro-zones” or strongly micro-textured regions, resulting in a significantly reduced fatigue life [13]. Therefore, a thorough understanding of the mechanisms of VS and the subsequent development of α texture is a primary requirement for microstructure control during processing and fabrication of titanium alloy components.

Substantial residual thermal stresses are present in titanium alloys even after stress-relief annealing treatment [14–16]. Moreover, defects such as dislocations generated during TMP in either β or $\alpha + \beta$ phase region act frequently as preferred nucleation sites for specific subsets of α variants [17–21]. Furthermore, the lattice distortion introduced within the β matrix by the precipitation of α phase introduces large local stress concentrations or “backstresses” which can influence VS within a local neighborhood [22–24]. Finally, for a polycrystalline aggregate under load (stress or strain), a highly heterogeneous stress field will develop. It is clear that the local stress state, due to a rich variety of sources, is a key factor in controlling VS and hence the final transformation texture during α precipitation in titanium alloys.

Because of the complicated interplay among different interacting factors, it is difficult to develop a fundamental understanding of VS by experimental study alone. Existing modeling attempts have considered only a limited number of these factors. For example, in the active slip model [18], the local Schmid factor is calculated for a given applied load with either the Sachs (homogeneous stress) or the Taylor (homogeneous strain) assumption. Since local stress and strain fields in a polycrystalline volume element vary significantly from grain to grain owing to the elastic anisotropy and inhomogeneity, active slip models offer only general trends and show limited agreement with experiments [25]. More complex criteria, involving interaction energy calculations using the transformation strain associated with the candidate variants and a threshold value have also been considered [26,27]. However, as the Sachs assumption is still employed in the interaction energy calculations, it was observed that the stresses imposed by the need to enforce strain compatibility at the interfaces can overwhelm the interaction energy and lead to other complications [28].

Using a three-dimensional (3D) quantitative phase field model [12], we have previously investigated the influence of a constant applied external strain and the transformation-induced internal stress on VS and microstructure evolution during $\beta \rightarrow \alpha$ transformation within a single parent β grain. However, the study of *variant selection in polycrystalline β volume elements* under the influence of stress faces three major challenges. First, one needs to determine the stress distribution in an elastically anisotropic and inhomogeneous polycrystalline β matrix under a given applied stress/strain condition. Second, one needs to describe nucleation and growth of coherent and semi-coherent α precipitates under the influence of such a highly non-uniform local stress field and to update the

stress field as the $\alpha + \beta$ microstructure evolves. Third, one needs to address VS of grain boundary α (GB α) by prior β grain boundaries and its influence on subsequent microstructure development into the interiors of adjacent β grains if the cooling rate is relatively low or the aging temperature is relatively high. In other words, the interplay between β grain boundaries and local stresses on VS and $\alpha + \beta$ microstructure evolution needs to be taken into account. The first two issues are the focus of the current study and the last one will be addressed in a separate paper.

Thus, the main objective of the current work is to explore the effects of different processing parameters on both microstructure and transformation texture evolutions due to local stress variations arising from elastic inhomogeneity in a polycrystalline β volume element. The major processing parameters considered are pre-strain or applied stress, boundary constraint and initial texture of the parent phase grains. The volume elements or simulation volumes investigated mimic microstructures sampled at different locations in a component, which may have experienced different thermal mechanical processing history and have different boundary constraints, and thus have different initial β phase textures and different internal stress/strain states.

The paper is organized as follows. In Section 2, we present an extension of a previously formulated 3D phase field model [12,29] to investigate both microstructure and texture evolution during α precipitation in polycrystalline titanium alloys. It is worth emphasizing that, based on gradient thermodynamics [30–32] and microelasticity theory [33–37], the phase field approach [38–44] (also called the diffuse-interface approach) offers an ideal framework to deal rigorously and robustly with the difficult challenges mentioned above. In particular, in combination with orientation distribution function (ODF) modeling [45] of simulated $\alpha + \beta$ microstructures, both micro- and macro-texture evolution accompanying the $\alpha + \beta$ microstructure evolution under different processing conditions can be documented. Two new parameters are also introduced to quantify the degree of variant selection (DVS) at the scale of both individual β grain (micro-DVS) and polycrystalline β volume element (macro-DVS) levels under different processing conditions. In Section 3, the model is employed to investigate VS behavior (i.e. degree of variant selection) under the influence of different aforementioned processing parameters and its effect on the evolution of both $\alpha + \beta$ microstructure and final α texture in polycrystalline volume element. Results are analyzed in Section 4 where VS behavior at the scale of individual β grain and polycrystalline β volume element levels is linked to the strength of final α texture. The main findings are summarized in Section 5.

2. Model formulation

In this section, we present an extension of a previously formulated 3D phase field model to investigate $\alpha + \beta$ microstructure during $\beta \rightarrow \alpha$ transformation in polycrystalline Ti–6Al–4V (in wt.%) volume elements under the influence of pre-strain $\bar{\epsilon}^{appl}$ or external stress σ^{appl} . The extended phase field model will also be coupled with an orientation distribution function model to analyze the response of transformation texture of the α phase to different processing parameters.

2.1. Polycrystalline β volume element

In the current work, we consider a polycrystalline volume element of the β phase that is formed by a periodical repetition of M different oriented β grains that occupy a computation cell of $128 \times 128 \times 128$. A crystallographic orientation of each β grain, $\mathbf{g} \in \frac{\text{SO}(3)}{G_\beta}$, is defined as a proper rotation that maps the macro-scale sample basis vectors onto the local crystal lattice basis. Here $\frac{\text{SO}(3)}{G_\beta}$ represents the fundamental zone of orientations for the cubic, β phase and is formally defined as the set of all left cosets of the symmetry subgroup, G_β , in the special orthogonal group of rotations in 3-dimensions, $\text{SO}(3)$. Being in proper rotation, \mathbf{g} can be represented as an 3×3 orthogonal matrix with determinant +1 [45]. A rotation matrix field $Q_{ij}(\mathbf{r})$ is then introduced to describe the polycrystalline structure [46], where $Q_{ij}(\mathbf{r})$ assumes a constant value \mathbf{g} within a grain but varies between β grains depending on its orientation. In practice, it is convenient to describe the orientation by a triplet of Euler angles, e.g. $\mathbf{g} = [\phi_1, \Phi, \phi_2]$ using Bunge notation [45].

2.2. Phase field model for α precipitation in an elastically and structurally inhomogeneous polycrystalline β volume element

2.2.1. Chemical free energy for polycrystalline systems

Arbitrary α/β two-phase microstructure in polycrystalline parent β volume element includes both structural and chemical non-uniformities. For the ternary Ti-Al-V system, two conserved phase field order parameters, i.e. concentration fields $X_k(\mathbf{r}) (k = \text{Al}, \text{V})$, are required to describe the chemical non-uniformities of solute components Al and V in the system. At the scale of individual γ th β grain, twelve non-conserved structural order parameters, $\phi_p(\gamma, \mathbf{r}) (p = 1, 2, \dots, N = 12)$, are needed to describe the structural non-uniformities associated with the total N orientation variants (OVs). One more dependent structural order parameter, $\phi_p(\gamma, \mathbf{r}) (p = 13)$, is also introduced to describe the spatial distribution of the matrix phase within γ th grain. In the frame work of the multi-phase field model, all such non-conserved order parameters are subjected to the constraint that $\sum_{p=1}^{N+1} \phi_p(\gamma, \mathbf{r}) = 1$ [47,48]. For a polycrystalline aggregate consisting of M β grains, the total number of non-conserved order parameters to describe the spatial distribution of α phase is $M \times 12$.

The total free energy of such a system having an arbitrary coherent or semi-coherent two-phase microstructure, including both chemical and structural non-uniformity, is formulated on the basis of the gradient thermodynamics [30]. The chemical free energy can be extended straightforwardly to the polycrystalline system from its counterpart for a single crystal as follows:

$$F^{\text{chem}} = \frac{1}{V_m} \int_V \left[G_m\{\mathbf{T}, X_k, \phi_p(\gamma)\} + \frac{\kappa_c}{2} \sum_{k=\text{Al,V}} |\nabla X_k|^2 + \frac{1}{2} \sum_{\gamma=1}^M \sum_{p=1}^N [\nabla \phi_p]^T \mathbf{k}_p(\gamma) [\nabla \phi_p] \right] dV \quad (1)$$

where κ_c and $\mathbf{k}_p(\gamma)$ are the gradient energy coefficient and gradient energy coefficient tensor characterizing contributions from non-uniformities in concentration and structure within a polycrystalline system, respectively. In particular, the variation of the structural order parameter across an

α/β interface represents the variation in the amount of shear or shuffle or both that are required to bring the bcc structure to the hcp structure across the interface following the Burgers path [8]. A set of eigenvalues for the $\mathbf{k}_p^c (p = 1, \dots, 12)$ tensors of all 12 variants has been employed to describe the interfacial energy anisotropy in the crystal reference frame [12]. In the sample reference frame, $\mathbf{k}_p(\gamma)$ is obtained via $[\mathbf{k}_p(\gamma)] = [\mathcal{Q}] [\mathbf{k}_p^c(\gamma)] [\mathcal{Q}]^T$ where \mathcal{Q} is the rotation matrix that describes the orientation of the γ th β grain. Note that T represents the system temperature.

The bulk chemical free energy density in Eq. (1) is expressed as:

$$\begin{aligned} G_m\{\mathbf{T}, X_k, \phi_p(\gamma)\} &= \sum_{\gamma=1}^M \sum_{p=1}^N h\{\phi_p(\gamma)\} G_m^\alpha\left(\mathbf{T}, X_{\text{Al,V}}^\alpha\right) \\ &\quad + \left[1 - \sum_{\gamma=1}^M \sum_{p=1}^N h\{\phi_p(\gamma)\} \right] G_m^\beta\left(\mathbf{T}, X_{\text{Al,V}}^\beta\right) \\ &\quad + \sum_{\gamma}^M \sum_{p=1}^N \sum_{q>p}^{N+1} \omega_{pq} |\phi_p(\gamma) \phi_q(\gamma)| \end{aligned} \quad (2)$$

where, $h\{\phi_p(\gamma)\} = \phi_p^3(\gamma)[6\phi_p^2(\gamma) - 15\phi_p(\gamma) + 10]$ is an interpolation function connecting the free energy surfaces (as function of concentration and temperature) of the α and β phase. The term $\sum_{p=1}^N \sum_{q>p}^{N+1} \omega_{pq} |\phi_p(\gamma) \phi_q(\gamma)|$ introduces a hump on the free energy surface between variants p and q , and hump height is proportional to $\omega_{pq} \cdot G_m^\alpha\left(\mathbf{T}, X_{\text{Al,V}}^\alpha\right)$ and $G_m^\beta\left(\mathbf{T}, X_{\text{Al,V}}^\beta\right)$ are the equilibrium molar free energies of α and β phases as a function of temperature and individual phase concentration $X_{\text{Al,V}}^\alpha$ and $X_{\text{Al,V}}^\beta$, respectively.

2.2.2. Strain energy of an elastically and structurally inhomogeneous system

A polycrystalline aggregate with $\alpha + \beta$ two-phase microstructure is a typical elastically and structurally inhomogeneous system. The system is characterized by an arbitrary distribution of the lattice misfit strain, $\epsilon_{ij}^T(\mathbf{r})$, (transformation strain due to α precipitation), and a heterogeneous distribution of elastic moduli $C_{ijkl}(\mathbf{r})$ due to different orientations of individual β grains, i.e., both $C_{ijkl}(\mathbf{r})$ and $\epsilon_{ij}^T(\mathbf{r})$ are functions of spatial coordinate \mathbf{r} . Elastic strain energy of such a system under an external loading or pre-strain, $E^{el}[C_{ijkl}(\mathbf{r}), \epsilon_{ij}^T(\mathbf{r})]$, is obtained using the iterative method developed by Wang et al. [49,50]. By introducing a virtual strain field $\epsilon_{ij}^0(\mathbf{r})$ and a reference modulus C_{ijkl}^0 , the exact elastic equilibrium, including total strain and stress distributions, of an elastically and structural inhomogeneous system are obtained [49,50] by solving the elasticity problem in an equivalent elastically homogeneous system. $\epsilon_{ij}^0(\mathbf{r})$ is an energy minimizer of the total strain energy functional that determines the equilibrium state of the elastically and structurally inhomogeneous system. In practice, it can be obtained numerically through a solution of the time-dependent Ginzburg–Landau type equation [49],

$$\frac{\partial \epsilon_{ij}^0(\mathbf{r}, \tau)}{\partial t} = -L_{ijkl} \frac{\delta E^{el}}{\delta \epsilon_{kl}^0(\mathbf{r}, \tau)} \quad (3)$$

where elastic strain energy of the system, E^{el} , is given by:

$$\begin{aligned} E^{el} = & \frac{1}{2} \int v \left[C_{ijmn}^0 \Delta S_{mnpq}(\mathbf{r}) \cdot C_{pqkl}^0 - C_{ijkl}^0 \right] \\ & \times (\varepsilon_{ij}^0(\mathbf{r}) - \varepsilon_{ij}^T(\mathbf{r})) \cdot (\varepsilon_{kl}^0(\mathbf{r}) - \varepsilon_{kl}^T(\mathbf{r})) d^3\mathbf{r} \\ & + \frac{1}{2} \int C_{ijkl}^0 \varepsilon_{ij}^0(\mathbf{r}) \varepsilon_{kl}^0(\mathbf{r}) d^3\mathbf{r} - \bar{\varepsilon}_{ij} \int C_{ijkl}^0 \varepsilon_{kl}^0(\mathbf{r}) d^3\mathbf{r} \\ & + \frac{V}{2} C_{ijkl}^0 \bar{\varepsilon}_{ij} \bar{\varepsilon}_{kl} - \frac{1}{2} \int \frac{d^3\mathbf{k}}{(2\pi)^3} n_i \tilde{\sigma}_{ij}^0(\mathbf{k}) \Omega_{jk}(\mathbf{n}) \tilde{\sigma}_{kl}^0(\mathbf{k}) * n_l \quad (4) \end{aligned}$$

where L_{ijkl} is the kinetic coefficient tensor (a convenient choice is $L_{ijkl} = L[C_{ijkl}^0]^{-1}$ [51]) and the parameter τ describes the elastic relaxation process. In Eq. (4), $\Delta S_{ijkl}(\mathbf{r}) = [C_{ijkl}^0 - C_{ijkl}(\mathbf{r})]^{-1}$. In order to ensure the convergence [52], $L[C_{ijkl}^0]^{-1}$ has been chosen to be $L[C_{ijmn}^0]^{-1} \Delta C_{mnlk}(\mathbf{r})$ during the iteration of Eq. (3). Elastic inhomogeneity $C_{ijkl}(\mathbf{r})$ defined in the sample reference is obtained by $C_{ijkl}(\mathbf{r}) = Q_{ip}^T(\mathbf{r}) Q_{jq}^T(\mathbf{r}) Q_{km}^T(\mathbf{r}) Q_{ln}^T(\mathbf{r}) C_{pqmn}^0$. Einstein's summation convention for repeated indices is assumed throughout. $\tilde{\sigma}_{ij}^0(\mathbf{k}) = C_{ijkl}^0 \tilde{\varepsilon}_{kl}^0(\mathbf{k})$, $\tilde{\varepsilon}_{ij}^0(\mathbf{k})$, is the Fourier transform of $\varepsilon_{ij}^0(\mathbf{r})$, $\Omega_{ij}^{-1}(\mathbf{n}) = C_{ijkl}^0 n_k n_l$, and the superscript asterisk denotes the complex conjugate. The last integral in Eq. (4) excludes a volume of $(2\pi)^3/V$ around the point at $\mathbf{k} = 0$. n_i is the i th component ($i = 1, 2, 3$) of a unit vector, $k_i/|\mathbf{k}|$, in the reciprocal space. The strain energy in the form in Eq. (4) is convenient when the body is fully clamped and thus its macroscopic deformation is specified by the pre-strain ε_{ij}^{-app} . The strain energy in Eq. (4) needs to be modified if the macroscopic deformation of the body is controlled by the applied external stress, σ_{ij}^{app} . In this case, the macroscopic shape is obtained by allowing the body to relax at fixed σ_{ij}^{app} to minimize the strain energy with respect to $\bar{\varepsilon}_{ij}$. The energy minimization is obtained with minimizer being $\bar{\varepsilon}_{ij} = \bar{\varepsilon}^0 + S_{ijkl}^0 \sigma_{kl}^{app}$, where $\bar{\varepsilon}_{ij}^0 = \int \varepsilon_{kl}^0(\mathbf{r}) d^3\mathbf{r}/V$.

From Eq. (4), it is obvious that the stress-free transformation strain $\varepsilon_{ij}^T(\mathbf{r})$ associated with α precipitates in the whole system is a critical input in formulating the strain energy for such an inhomogeneous system. In the sample reference frame, $\varepsilon_{ij}^T(\mathbf{r})$ is formulated upon spatial distribution of the transformation strain field:

$$\varepsilon_{ij}^T(\mathbf{r}) = \sum_{\gamma=1}^M \sum_{p=1}^N \varepsilon_{ij}^{000}(\gamma, p) \times \phi_p(\gamma, \mathbf{r}) \quad (5)$$

as a linear combination of individual structural order parameters within each β grain, $\phi_p(\gamma, \mathbf{r})$.

$\varepsilon_{ij}^{000}(\gamma, p)$ is the SFTS tensor of p th α variant in γ th β grain expressed in the sample reference frame. It can be obtained through $\varepsilon_{ij}^{000}(\gamma, p) = Q_{ik}(\gamma) \varepsilon_{ik}(\gamma) \varepsilon_{kl}^{00}(p) Q_{jl}^T(\gamma)$, where $\varepsilon_{ij}^{00}(p)$ denotes the SFTS tensor of the p th α variant in the crystal reference frame.

Thus, the elastic equilibrium is obtained through the converged value of the virtual misfit strain $\varepsilon_{ij}^0(\mathbf{r})$ in Eq. (3). Then, the total strain in the system is:

$$\varepsilon_{ij}(\mathbf{r}) = \bar{\varepsilon}_{ij} + \frac{1}{2} \int \frac{d^3\mathbf{k}}{(2\pi)^3} [n_i \Omega_{jk}(\mathbf{n}) + n_j \Omega_{ik}(\mathbf{n})] \tilde{\sigma}_{kl}^0(\mathbf{k}) n_l e^{i\mathbf{k}\cdot\mathbf{r}} \quad (6)$$

and the stress distribution $\sigma_{ij}(\mathbf{r})$ in the polycrystalline system can be obtained through $\sigma_{ij}(\mathbf{r}) = C_{ijkl}^0 [\varepsilon_{kl}(\mathbf{r}) - \varepsilon_{kl}^0(\mathbf{r})]$. The elastically and structurally inhomogeneous polycrystalline β volume element during α precipitation is then equivalent to an elastic homogeneous system with modulus C_{ijkl}^0 with the equilibrium internal stress distribution described by Eq. (3).

2.2.3. Kinetic equations

The temporal and spatial evolutions of both concentration and structural order parameters, i.e. microstructure evolution, are governed by the Cahn–Hilliard equation and the time-dependent Ginzburg–Landau equation (TDGL), respectively. For simplicity, the diffusion along grain boundaries is treated identically as bulk diffusion. The diffusion equation is the same as that within a single grain [12], i.e.

$$\frac{1}{V_m^2} \frac{\partial X_k(\mathbf{r}, t)}{\partial t} = \nabla \sum_{j=1}^{n-1} M_{kj}(T, X_i, \phi_j) \nabla \frac{\delta F}{\delta X_j(\mathbf{r}, t)} + \zeta_k(\mathbf{r}, t) \quad (7)$$

There are total $M \times N$ independent order parameters for α precipitates in the polycrystalline system and the governing equation is given as [46]:

$$\begin{aligned} \frac{\partial \phi_p(\gamma, \mathbf{r}, t)}{\partial t} = & \varphi(\gamma, \mathbf{r}) \left\{ -L_\phi \left[\frac{1}{\bar{N}} \sum_{p \neq q} \left(\frac{\delta F}{\delta \phi_p(\gamma, \mathbf{r}, t)} - \frac{\delta F}{\delta \phi_q(\gamma, \mathbf{r}, t)} \right) \right. \right. \\ & \left. \left. + \frac{\delta E^{el}}{\delta \phi_p(\gamma, \mathbf{r}, t)} \right] + \zeta_p(\mathbf{r}, t) \right\} \quad (8) \end{aligned}$$

where $\varphi(\gamma, \mathbf{r})$ defines the shape of the individual β grain that is equal to unity inside the γ th β grain and vanishes outside of it. $M_{kj}(T, X_i, \phi_j)$ denotes the chemical mobility, L_ϕ is the mobility of the structural order parameters characterizing interface kinetics, and ζ_k and ζ_p are the Langevin noise terms for composition and the long-range order parameter, respectively. In Eq. (8), \bar{N} is the number of phases that co-exist locally [48].

It needs to be mentioned that the variation of the strain energy with respect to order parameter is calculated based on the assumption that elastic relaxation occurs much faster than α precipitation. That is, Eq. (3) is first solved to obtain a steady-state solution for the virtual strain $\varepsilon_{ij}^0(\mathbf{r})$ with a clamped order parameter and concentration field. In addition, it is also assumed that, during α precipitation, there would be no grain growth within the polycrystalline β volume element. The effective strain and inhomogeneous elastic modulus $C_{ijkl}(\mathbf{r})$ is then treated as a constant in the calculation of the functional variation of the strain energy with respect to the order parameter field $\phi_p(\gamma, \mathbf{r})$.

$$\frac{\delta E^{el}}{\delta \phi_p(\gamma, \mathbf{r})} = \frac{1}{2} \frac{\delta \left\{ \int_V (C_{ijmn}^0 \Delta S_{mnpq}(\mathbf{r}) \cdot C_{pqkl}^0 - C_{ijkl}^0) \times (\varepsilon_{ij}^0(\mathbf{r}) - \varepsilon_{ij}^T[\phi_p(\gamma, \mathbf{r})])(\varepsilon_{kl}^0(\mathbf{r}) - \varepsilon_{kl}^T[\phi_p(\gamma, \mathbf{r})]) d^3\mathbf{r} \right\}}{\delta \phi_p(\gamma, \mathbf{r})} \quad (9)$$

All model parameters and materials properties can be referred to Ref. [12].

2.3. Transformation texture of α phase in polycrystalline β volume element via orientation distribution function analysis

To permit a quantitative description of textures for both phases and evolution of transformation texture, it is necessary to describe the orientation density of each phase in an appropriate 3-D representation, that is, in terms of its ODF [53]. The ODF is defined as a probability density function of orientation \mathbf{g} that models the relative frequencies of crystal orientations within the specimen by volume [45]. Mathematically, the ODF $f(\mathbf{g})$ is defined by the following relationship:

$$\frac{dV}{V} = f(\mathbf{g})d\mathbf{g} \quad (10)$$

where V is the sample volume and dV is the volume of all crystals with the orientation \mathbf{g} in the angular element $d\mathbf{g}$. To be specific, $d\mathbf{g} = 1/8\pi^2 \sin(\Phi) d\phi_1 d\Phi d\phi_2$ is the volume of the region of integration in orientation space $[\phi_1, \Phi, \phi_2]$. Choice of $d\mathbf{g}$ such that $\int f(\mathbf{g})d\mathbf{g} = 1$ to normalize the ODF implies that the uniform random (UR) ODF, $f_{\text{UR}}(\mathbf{g}) \equiv 1 \forall \mathbf{g}$, which is consistent with the custom of expressing $f(\mathbf{g})$ in terms of multiples of the UR ODF (m.r.d.).

Lattice orientation analysis on the simulation volumes is accomplished by reading the orientation information from the simulation into the MTEX (Matlab Toolbox for Quantitative Texture Analysis) [54] as a virtual electron back-scattered diffraction (EBSD) scan. A total of 128^3 individual orientations are measured. The orientations of all individual α phases are also measured by the EBSD scan according to the orientation of their matrix β grain and the BOR [55]. In order to be as objective as possible, MTEX automatic kernel density estimation was employed for computing orientation distribution functions from the virtual EBSD data [53]. The chosen kernel is a de la Vallée Poussin kernel with a smoothing half-width of 5 deg.

Experimentally, crystallographic preferred orientation is also frequently expressed by the pole density function (PDF) P . The PDF of a specimen models the relative frequencies of specific lattice plane orientations h within the specimen volume. To be specific, a pole that is defined by the direction y in a given 2D pole figure, $P_h(y)$, corresponds to a region in the 3D-ODF $f(\mathbf{g})$ that contains all possible rotations with angle θ about this direction y in the pole figure. $P_h(y) = \frac{1}{2\pi} \int_{\theta=0}^{2\pi} f(\mathbf{g})d\theta$ where y is the position of a given pole on the reference sphere [53]. Pole figures for a set of planes of interest can be readily obtained from a given ODF. For convenience, the freely available MTEX [54] is utilized to make all pole figures.

2.4. Quantify degree of variant selection (DVS)

As will be shown in the following sections, the differences in both $\alpha + \beta$ microstructure and transformation texture of α phase result from the occurrence of different DVS at the scales of both individual β grain and polycrystalline volume element levels under different processing conditions. It is thus required to estimate DVS quantitatively at these two scales.

2.4.1. Macro-DVS at polycrystalline volume element

Over a polycrystalline volume element, the macro-DVS essentially characterizes the level of similarity between a given orientation distribution associated with observed α phase, $f(\mathbf{g})$, from the one $f_0(\mathbf{g})$ without VS, i.e. the orientation density of β phase texture is inherited equally by all 12 α variants within each grain [18,56–58]. Thus, the macro-DVS can be quantified by the ratio:

$$F_{\text{VS}} = F/F_0 \quad (11)$$

where $F = \int_{SO(3)} f^2(\mathbf{g})d\mathbf{g}$ is the so called texture index [45] that quantifies the texture sharpness or strength, F_0 is the texture index of the α phase texture without VS. F ranges from 1 (for the uniform distribution $f_{\text{UR}}(\mathbf{g})$) to infinity. Similarly, $F_{\text{VS}} \equiv 1$ if no VS occurs and $F_{\text{VS}} > 1$ when VS occurs. Analogous to the texture index that is a measure of the deviation from the uniform distribution, F_{VS} provides a measure of the degree of deviation from the texture without VS.

2.4.2. Micro-DVS within individual β grain

In order to draw connections between VS behaviors within individual β grains and the overall polycrystalline β volume element, it is necessary to quantify DVS within individual parent β grains. It is known that among all 12 α variants, there are only 6 types of possible misorientation relationships (MRs) between any two variants [59]. As, shown in Fig. 1(a) when represented as misorientation/axis pair, all 6 types of MR are, I (Identity), $10.5^\circ/[0001]_x$, $60^\circ/[11\bar{2}0]_z$, $60.83^\circ/[-1.38, -1, 2.38, 0.36]_z$, $63.26^\circ/[10, 5, 5, \bar{3}]_z$, $90^\circ/[1, -2.38, 1.38, 0]_z$, referred to as Type I to Type VI MRs, respectively. Provided no VS, the occurrence frequencies $f_i^{\text{Random}}(i = 1..6)$ of each MR are 12, 6, 12, 24, 12 and 12 out of all 78 possible pair-wise combinations [59,60] within a single β grain when doing uncorrelated misorientation analysis, i.e. two variants are not necessary in contact with each other. The measured uncorrelated misorientation distribution $f_i^{\text{PF}}(i = 1..6)$ can be compared with the random occurrences to evaluate the degree of deviation from it. Thus, the micro-DVS within individual i th β grain, R_{VS}^i , can be quantified by the summation of the deviation of each type of MR from its random occurrences:

$$R_{\text{VS}}^i = \sum_{j=1}^6 |f_j^{\text{PF}} - f_j^{\text{Random}}| \quad (12)$$

The physical meaning of R_{VS}^i can be interpreted as: provided no VS, there will be no deviation from random occurrence frequencies for each type of misorientation, i.e. $R_{\text{VS}}^i \equiv 0$ (Fig. 1(b)); if a single variant is able to percolate through a whole single β grain, maximum degree of VS is reached with $R_{\text{VS}}^i \equiv 1.6922$, as shown in Fig. 1(c). Thus, the value of R_{VS}^i is able to characterize quantitatively DVS within the i th β grain. The computation of an uncorrelated misorientation distribution from the EBSD data of all individual α variants in a parent β grain is performed using MTEX [54].

3. Results

3.1. Starting β phase polycrystalline microstructure and texture

A polycrystalline volume element of Ti–6Al–4V (Fig. 2(a)) is first created by the Voronoi algorithm [61]

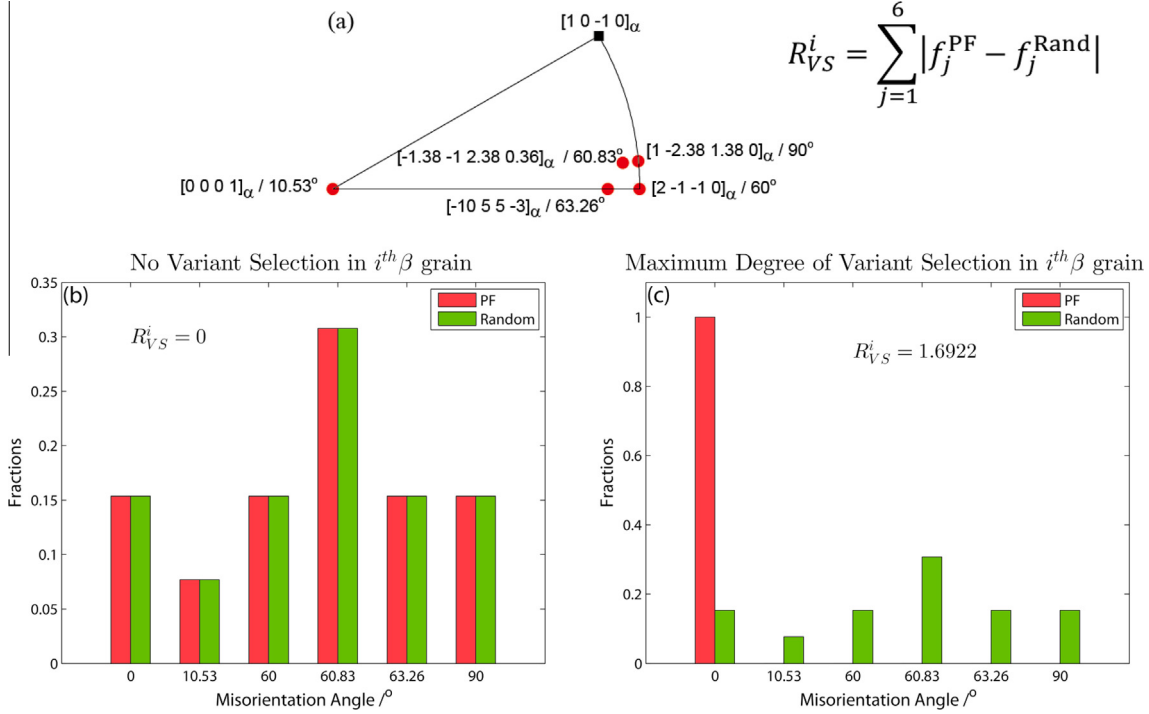


Fig. 1. (a) All possible misorientation relationships between different pairs of α/α variants. Misorientation axes are expressed in a standard triangle for hcp structure; uncorrelated misorientation analysis for observed (either experimental or simulated, represented as red bars) $\alpha + \beta$ microstructure (b) without variant selection and (c) with maximum degree of variant selection within an individual β grain where a single variant percolates the whole β grain. Green bars in (b) and (c) denote theoretical misorientation distribution in the case of no VS. (For interpretation of the references to color in this figure legend, the reader is referred to the web version of this article.)

and further relaxed by a phase field grain growth code [62] to obtain equilibrium junctions among β grains. The β texture is then represented by $\{101\}_\beta$ pole figures as shown in Fig. 2(b). Since the starting texture of the β grains has been found to have a strong influence on the transformation texture of α variants because of the Burgers orientation relationship between the two phases [57], two sets of initial orientations of the β grains are considered in the current study. One is populated with orientations sampled from a uniform random texture referred to as the “RT” sample and the other has grains sampled from a strong cube texture as the “ST” sample. Their textures are represented by the $\{101\}_\beta$ pole figures shown in Fig. 2(b) and (c), respectively. Due to the limited number of grains in the volume elements the pole intensities are quite high even for the RT sample, however the ST sample has a relatively larger maximum pole intensity of the $\{101\}_\beta$ pole than that of the RT one. In addition, the texture index F for the ST sample is $50.38 \times \text{m.r.d.}^2$, while that for the RT sample is $22.38 \times \text{m.r.d.}^2$, which further distinguishes the texture of the two simulation volumes despite containing a very limited number of grains.

3.2. Evolution of $\alpha + \beta$ microstructure and transformation texture during α precipitation

Evolution of the $\alpha + \beta$ microstructure during α precipitation is obtained by solving simultaneously Eqs. (7) and (8). In the case of a clamped boundary without any pre-strain (referred to as Fix-End) the microstructure evolution in the RT sample during α precipitation is shown in Fig. 3. The red color represents the α phase and the semi-transparent light-blue color represents the matrix β

phase. The white lines indicate β grain boundaries. It is clear that the α phase nucleates homogeneously throughout the whole polycrystalline volume element as shown in Fig. 3(b) and (c).

In order to quantify the texture evolution during α precipitation, a virtual EBSD scan is performed through the sample to read in orientation information of individual α precipitates according to the index of the α variants [12] and orientation of the matrix β grains based on BOR [55]. The ODFs for the α phase are obtained using the same approach as that used in describing the β texture [63]. The α textures are represented by the $\{0001\}_\alpha$ pole figures as shown in Fig. 3(a')–(c'). By comparing with the $\{101\}_\beta$ pole figure of the starting texture of the β grains (Fig. 2(b)), the α pole figures have similar maximum intensity locations, indicating that the two phases maintain the BOR during precipitation. The strength of the transformed α texture can be represented by the texture-component maxima in these pole figures. For example, it is found that the strength of transformation texture of the α phase, represented by the maximum pole intensity in the $\{0001\}_\alpha$ pole figure, has increased from 10.04 to $10.45 \times \text{m.r.d.}$ after aging (Fig. 3(a')–(c')). Also noticed is that the maximum intensity in the $\{0001\}_\alpha$ pole is larger than that in the $\{101\}_\beta$ pole (Fig. 2(c)), which suggests that variant selection may have occurred [64].

3.3. Effect of pre-strain on $\alpha + \beta$ microstructure and transformation texture evolution

In the RT sample, when a pre-strain is introduced by a compressive stress of 50 MPa that is applied along the x-axis of the sample before the system's boundary is

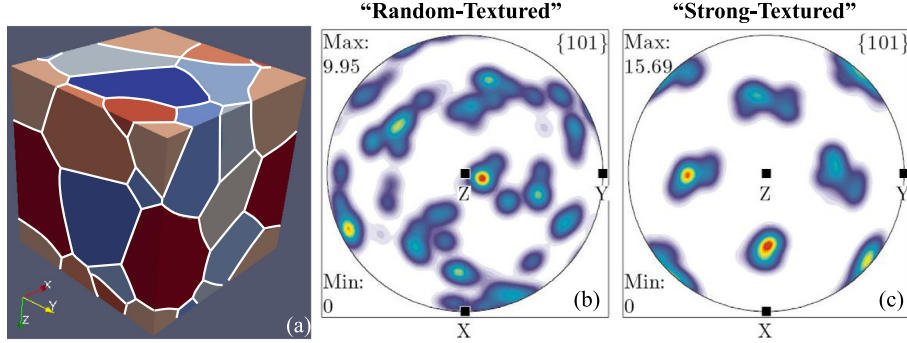


Fig. 2. (a) Polycrystalline volume element of the β phase with different strengths of texture, i.e., (b) a random-textured (RT) and (c) a strong-textured (ST) β sample, according to the maxima intensity in the $\{101\}_{\beta}$ pole figures.

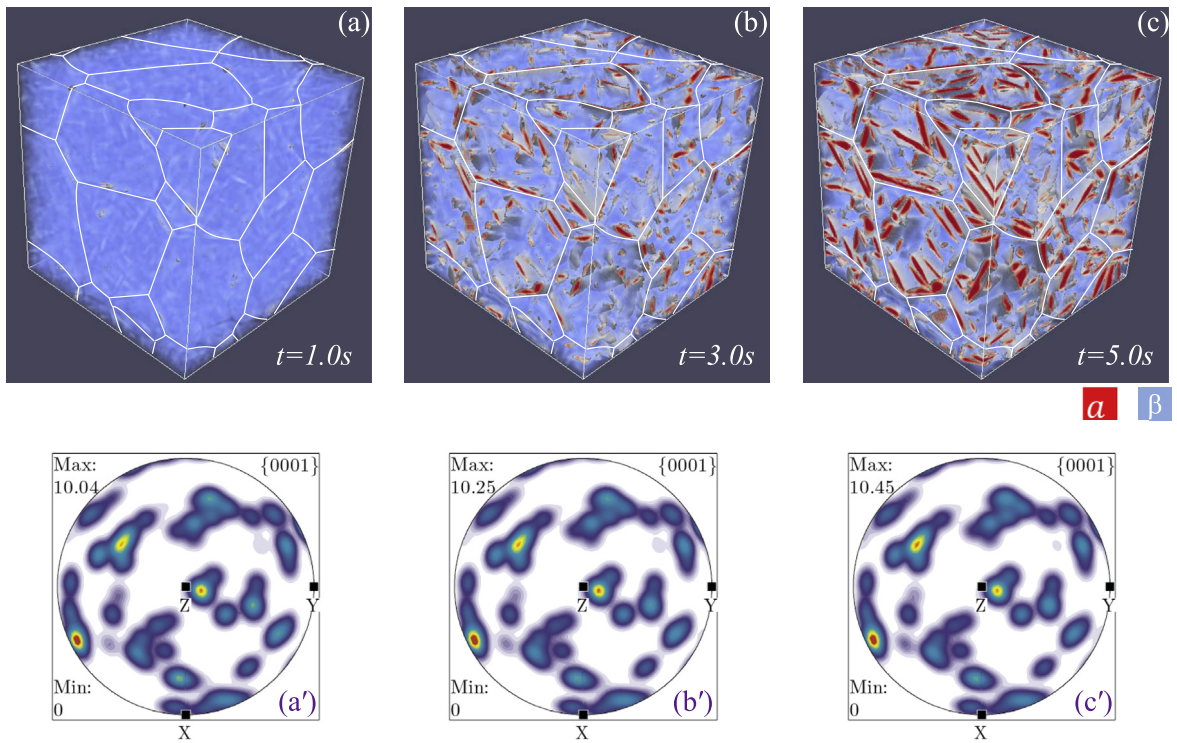


Fig. 3. (a)–(c) Microstructure evolution during α precipitation in the RT β sample without any pre-strain; (a')–(c') The corresponding α phase texture evolution represented by $\{0001\}_z$ pole figures.

clamped, nucleation of the α phase in different grains tends to occur at grain boundaries as shown in Fig. 4(a). Formation of closed-triangle patterns is observed, as indicated by arrows in Fig. 4(c) and (d). The precipitation kinetics varies significantly from one β grain to another. For example, in some grains, multiple α variants are formed simultaneously, while in others only a limited number of α variants survive. The corresponding transformation texture evolution of the α phase represented by the $\{0001\}_z$ pole figures is shown in Fig. 4(a')–(d'). When compared with the $\{101\}_{\beta}$ pole figures of the starting β grains (Fig. 2(b)), the α pole figures have much fewer intensity maxima. In particular, there are clear quantitative differences in the intensities at specific locations, which suggest that the parent texture of β phase are inherited by only limited numbers of α variants in different β grains. The strength of the transformation texture is

found to decrease when the α precipitation proceeds. The maximum intensity in the $\{0001\}_z$ pole figures decreases from $39.05 \times \text{m.r.d.}$ at 1.5 s to $23.2 \times \text{m.r.d.}$ at 9.0 s. In the meantime, several new orientations appear during α precipitation as indicated by the red arrows in Fig. 4(b')–(d'). The evolution of the α texture suggests that more orientation variants of the α phase form during α precipitation.

For the RT sample, different pre-strains have been introduced to investigate their influences on both the $\alpha + \beta$ microstructure and final α texture. Pre-strains are generated by applying a 50 MPa tensile/compressive stress along the x and z directions of the sample, referred to as X -Comp, X -Tensile, Z -Comp, and Z -Tensile, respectively. As can be seen clearly from Fig. 5(a)–(d), when subjected to different pre-strains, the final $\alpha + \beta$ microstructure obtained at

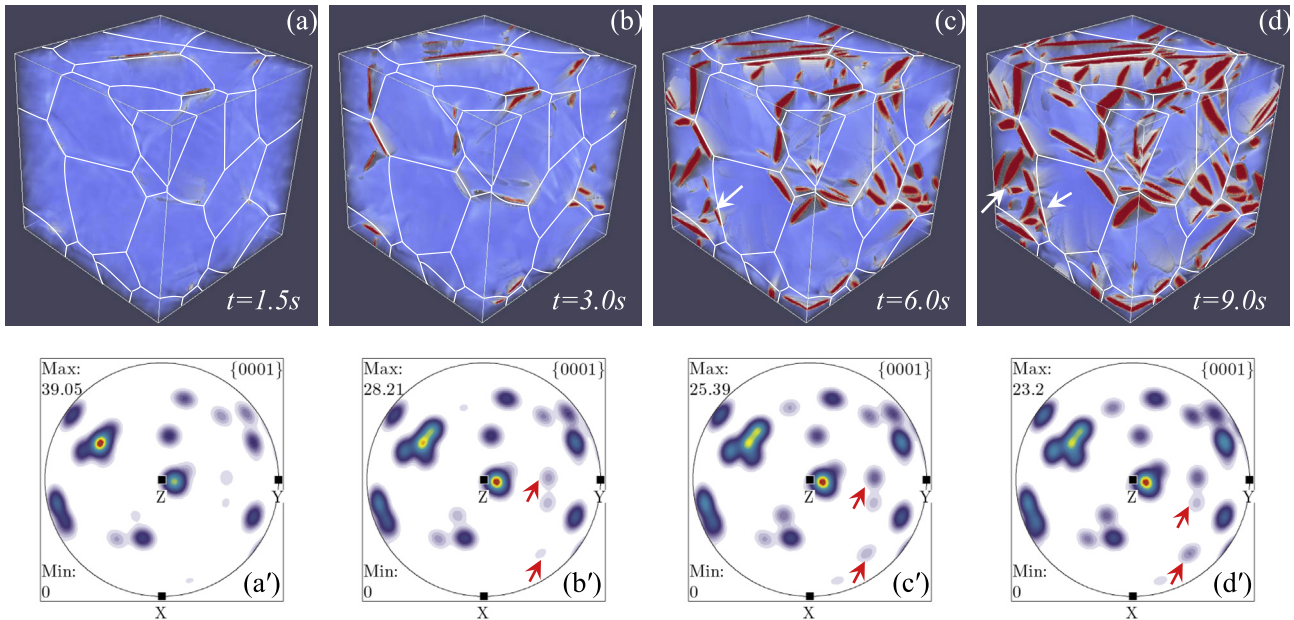


Fig. 4. (a)–(d) Microstructure evolution during α precipitation in the RT β sample under a pre-strain; (a')–(d') The corresponding α phase texture evolution represented by $\{0001\}_{\alpha}$ pole figures. The pre-strain is obtained by applying a 50 MPa compressive stress along the x -axis of the system.

$t = 10.0\text{ s}$ is quite different in terms of numbers and types of α orientation variants within individual β grains. So do the final α textures in terms of numbers of intensity maxima and the locations of the maxima, as shown in Fig. 5(a')–(d').

3.4. Effect of starting β phase texture on $\alpha + \beta$ microstructure and transformation texture evolution

Both size and texture of β grains will change due to grain growth or recrystallization in the β phase region [14,64] before temperature passes below the β transus. Thus, VS behavior needs to be understood according to the specific texture of β grains right prior to α precipitation. To focus on this effect, we consider a ST sample (Fig. 2(c)) that has the same grain geometry as that of the RT sample. Pre-strains are also generated by applying a 50 MPa tensile/compressive stress along the x and z directions of the sample, which are also referred to as X -Comp, X -Tensile, Z -Comp, and Z -Tensile, respectively. Similar to the results obtained from the RT sample, numbers and types of α orientation variants are found to vary at both individual β grain and overall polycrystalline volume element levels in the ST sample subjected to different pre-strains, as shown in Fig. 6(a)–(d). The final α textures in terms of the number and location of the maximum intensities are also more sensitive to the types of pre-strain, as shown in Fig. 6(a')–(d'). Evolution of the texture strength represented by the texture index F in both the RT and ST samples is shown in Fig. 7(a) and Fig. 7(b), respectively. In addition, the texture indices of the final α precipitate microstructures in both the RT and ST samples under different pre-strain conditions are represented respectively by the red and green bars in Fig. 7(c). It is found that, when subjected to a pre-strain, F of α texture will decrease gradually when α precipitation proceeds, at different rates depending on both the texture of the starting β grains and the type of the pre-strain. Moreover, the final α texture will always be stronger provided the presence of a pre-strain during α precipitation, irrespec-

tive of the strength of texture of the starting β grains. It is also noticed that, for both the RT and ST samples, α texture with a relatively large F at the initial stage of α precipitation could end up with a relatively small F , see, e.g., in the Z -Tensile case. Since the α phase acquires a specific texture from the texture of the β phase during the $\beta \rightarrow \alpha$ phase transformation through the BOR, it is generally believed that the stronger is the starting β phase texture, the stronger will be the final α phase texture, which is also true in most of the cases considered in our simulations. However, when the pre-strain is generated via a 50 MPa tensile stress, the texture index of the final α phase texture in the ST sample is smaller than that of the RT sample, as shown in Fig. 7(c) (X -Tensile). The degrees of VS quantified by F_{VS} under different pre-strains and starting β phase texture are summarized in Fig. 8(a). As can be readily seen, F_{VS} of the ST sample is smaller than that of the RT sample. Thus, when subjected to a certain pre-strain, the ST sample could have more α variants precipitating out simultaneously. It should also be noted that, even though with a smaller DVS, the ST samples still end up with stronger transformation textures except for the X -Tensile case (Fig. 7(c)).

3.5. Effect of boundary constraint on degree of variant selection

All the above simulations are performed for clamped samples. Such a boundary constraint has been referred to as *strain-constraint* [65] or *Fix-End* [64]. In practice, another type of commonly seen boundary constraint is that the system is subjected to a constant external load with freely moving boundaries. Such a constraint is referred to as *stress-constraint* [65] or *Free-End* [64]. Under the Free-End boundary condition (BC), F_{VS} under different external loads and starting β phase textures are summarized in Fig. 8(b). As compared to Fig. 8(a), F_{VS} is, in general, larger when the β sample is subjected to the Free-End BC. It is also observed that F_{VS} is not always smaller in the ST sample under the Free-End BC.

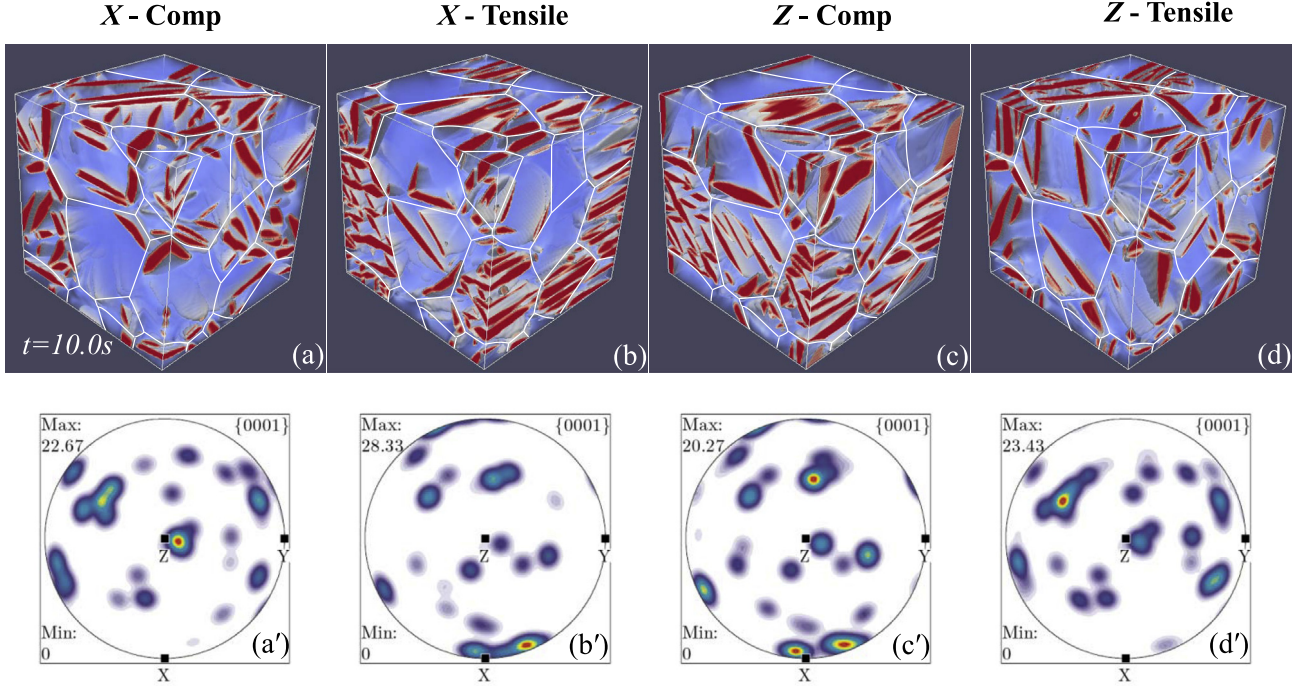


Fig. 5. (a)–(d) Final α/β microstructure in the RT β sample under different pre-strains; (a')–(d') The corresponding final α phase texture.

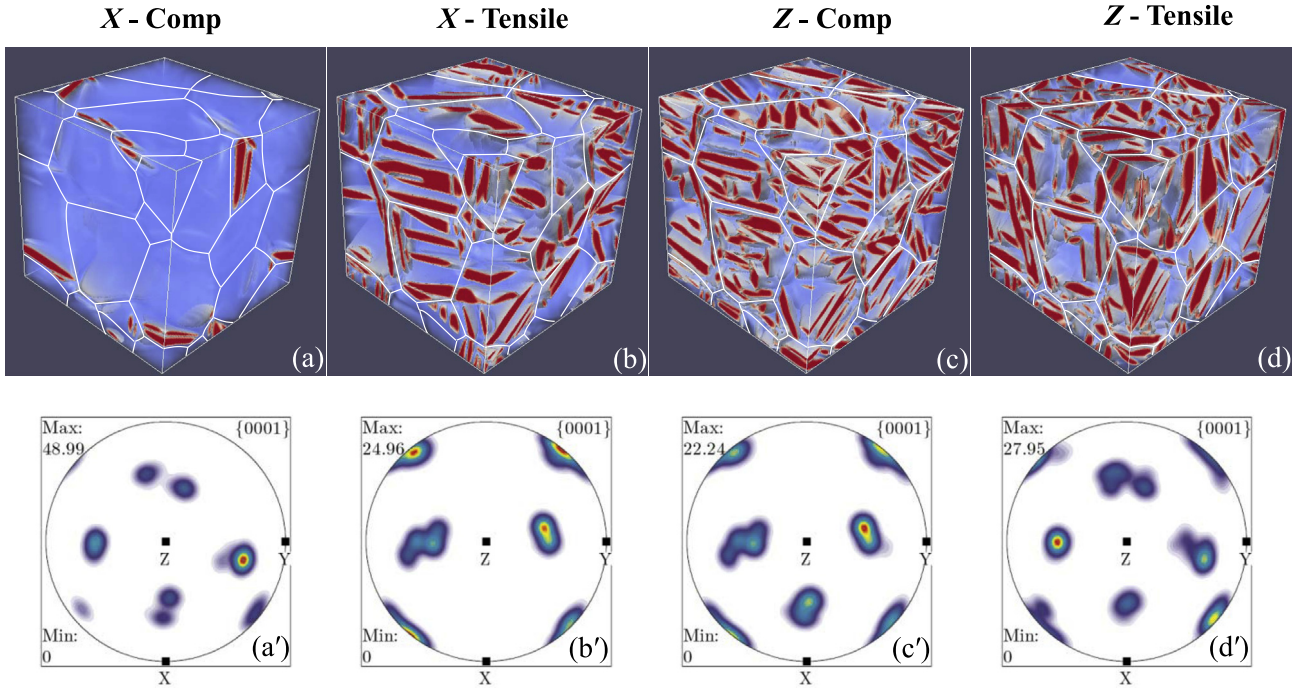


Fig. 6. (a)–(d) Final α/β microstructure in a ST β sample under different pre-strains; (a')–(d') The corresponding final α phase texture.

3.6. Connections between variant selection behaviors within individual β grain and polycrystalline volume element

It has been demonstrated above that the macro-DVS, F_{VS} , and strength of the α phase texture, F , are sensitive to processing variables such as the type of pre-strain, boundary constraint and strength of starting β phase texture. In order to draw connections of VS behaviors within

individual β grains and the overall polycrystalline β sample, the micro-DVS, R_{VS}^i , is calculated. Then F_{VS} is compared with the cumulative behavior of micro-DVS within all individual β grains, i.e., $\sum_i R_{VS}^i \times V_i$, where V_i denotes the volume fraction of the i th β grain. Results are presented in Fig. 9(a) and (b) for the RT and ST β samples, respectively. They show that the larger the $\sum_i R_{VS}^i \times V_i$ is, the larger the F_{VS} will be. Thus, F_{VS} is essentially a statistical measure

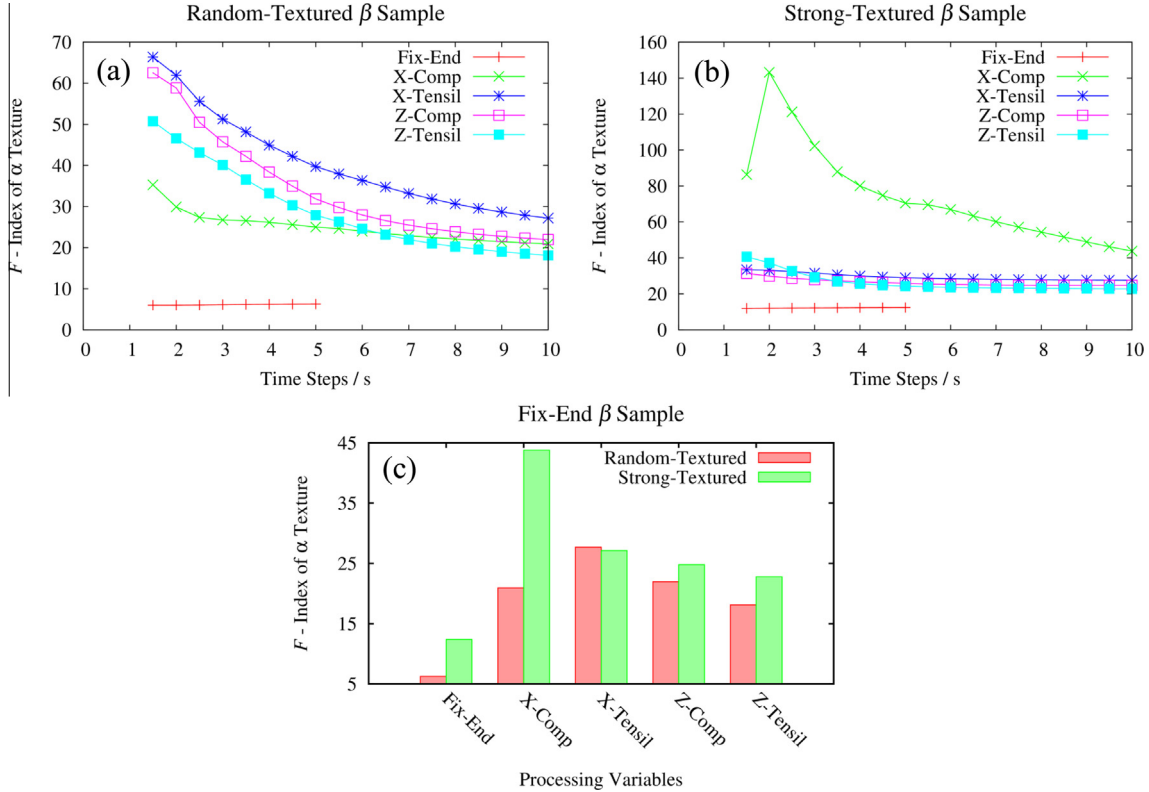


Fig. 7. (a) Texture index, F , of α phase texture as a function of time in the RT β sample under different pre-strains, (b) texture index of α texture as a function of time in the ST β sample under different pre-strains, (c) comparison of strength of final α phase texture quantified by texture index F .

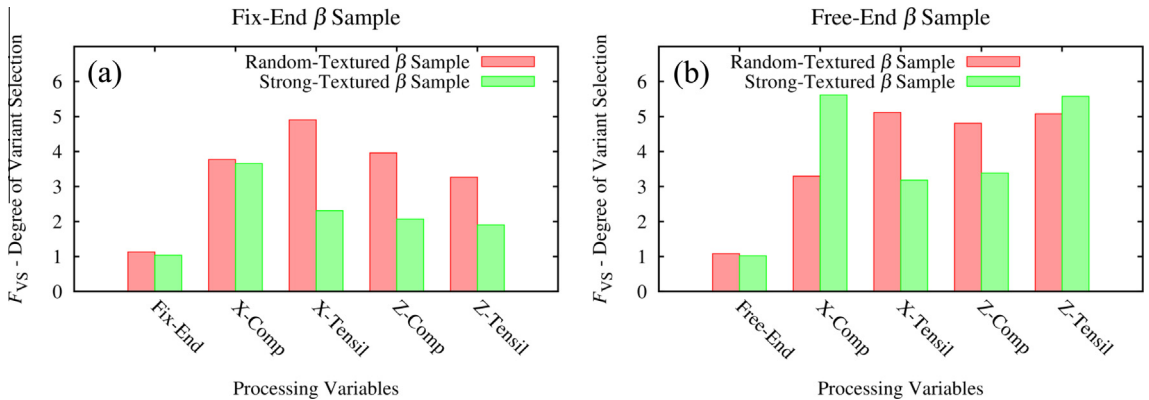


Fig. 8. Degree of variant selection, F_{VS} , in RT and ST β samples under different pre-strains (a) and external loadings (b).

accounting for the occurrence of different degrees of VS within all individual β grains. The responses of the micro-DVS to different processing parameters and their contributions to the macro-DVS are summarized and analyzed as follows:

3.6.1. Effect of processing condition on micro-DVS

First of all, the β samples under X -Tensile pre-strain (Fix-End) and external loading (Free-End) are used as examples to demonstrate the effect of boundary constraint and strength of starting β phase texture on R_{VS}^i . As can be seen from Fig. 10(a) and (b), when subjected to different boundary constraints, the differences in R_{VS}^i are more significant in the ST sample. This trend also holds when the sample is subjected to X -Comp pre-strain (Fig. 10(e) and (f)).

Thus, R_{VS}^i in the ST β sample is more sensitive to the boundary constraint than that in the RT sample.

As shown in Fig. 10(c), when the β sample is subjected to X -Tensile pre-strain, R_{VS}^i is significantly smaller in the ST sample than that in the RT sample in most of the prior β grains. Thus, when subjected to a specific pre-strain, the ST sample could have more α variants forming simultaneously (i.e. relatively small R_{VS}^i) within the majority of β grains, resulting in a relatively weak macro-texture (see Fig. 7(c) X -Tensile). However, as can be seen in Fig. 10(e), the trend is not followed when the β sample is subjected to X -Comp pre-strain, and R_{VS}^i in some prior β grains is significantly larger within the ST sample than that within the RT sample, resulting in a much stronger α phase texture inherited from the ST sample (see Fig. 7(c), X -Comp).

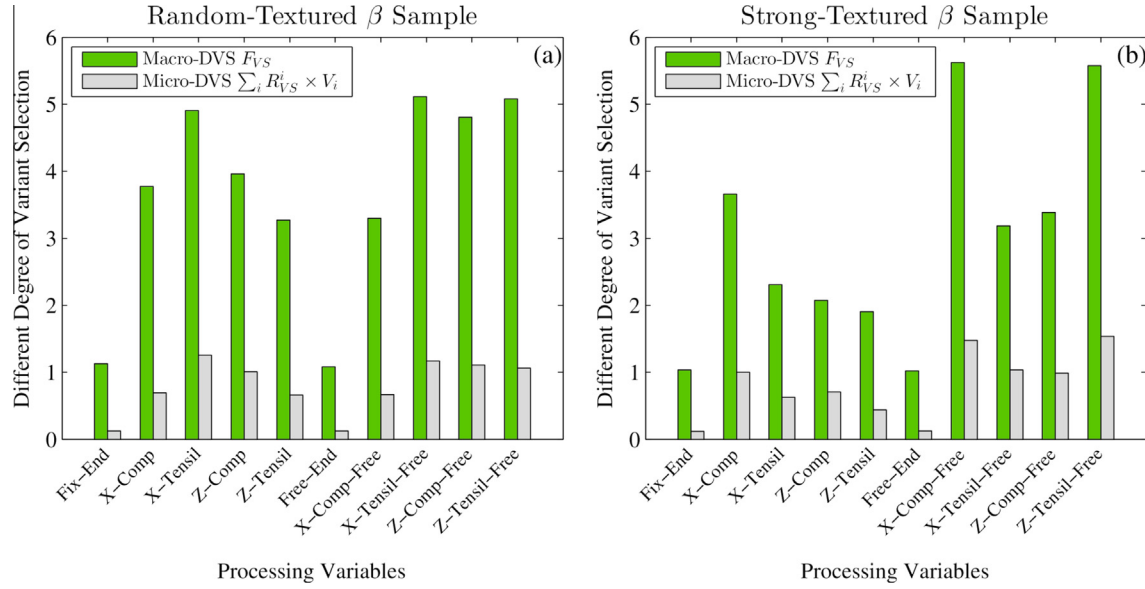


Fig. 9. Connections between macro-DVS and micro-DVS, $\sum_i R_{VS}^i \times V_i$, in both random-textured and strong-textured β samples under different processing conditions. Fix-End and Free-End denote clamped and relaxed boundary conditions (BCs), respectively. X-Comp-Free represents external loading along X-direction of the sample under the Free-End BC.

In the case of the X-Tensile external loading, R_{VS}^i in most of the prior β grains is also smaller in the ST sample than that in the RT sample, as shown in Fig. 10(d). However, the differences in R_{VS}^i between the RT and ST samples are not as significant as those when the β sample is subjected to Fix-End constraint with X-Tensile pre-strain (Fig. 10(c)).

When the β sample is subjected to X-Comp external loading, it is noticed that R_{VS}^i in each prior β grain is significantly larger in the ST sample than that in the RT sample (Fig. 10(f)). It is also noticed that under the Free-End BC R_{VS}^i is significantly larger when the β sample is subjected to X-Comp loading than that when the sample is subjected to X-Tensile loading (Fig. 10(d) and (f)).

3.6.2. Random-textured β sample under X-Tensile pre-strain

Considering the RT sample under X-Tensile pre-strain as an example, microstructures in the 2nd and 5th β grains are shown in Fig. 11(a) and (b), respectively. The volume fraction of each variant as a function of time within these two β grains is shown in Fig. 11(c) and (d), respectively. It is clear that there are more than 4 (V12, V5, V9, V3, and V11, in order of their volume fractions) variants selected in the 2nd β grain and, in contrast, only two variants (V8 and V12) are selected in the 5th grain. The micro-DVS values in the 2nd and 5th β grains are $R_{VS}^2 = 0.467$ and $R_{VS}^5 = 1.365$, respectively, indicating quite different VS behaviors within the two prior β grains. Since variant selection is sensitive to the local stress state within individual β grains [12], the local stress field (represented by σ_{11} expressed in the sample reference frame) within the two β grains before the transformation are calculated and shown in Fig. 11(e) and (f). As can be seen, the local stress states within the two β grains are not only non-uniform as indicated by the inset color bar, but also dramatically different from the external loading ($\sigma_{11} = 50$ MPa) that generates the pre-strain. In order to quantify the effect of external loading on selective nucleation and growth of specific α variants, interaction energy density between local stresses

from the initial external loading and each α variant under both coherent and semi-coherent states within the two β grains are calculated and the results are presented in Fig. 11(g) and (h), respectively. As expected from the interaction energy analysis, a uniform external loading can result in significant different variant selection behavior within different β grains. In the 2nd β grain, the favored variants are variants V3–V6, and V9–V12 at both nucleation and growth stages; while in the 5th β grain, the most favored ones are variants V2, V6, V8 and V12. Nevertheless, from the volume fraction analysis of the phase field simulation results, variants V12, V5, V9, V3, and V11 are selected in the 2nd β grain and only variants V8 and V12 are selected in the 5th β grain. Within the two prior β grains, only a fraction of all favored variants by the external loading is selected.

3.6.3. Strong-textured β sample under X-Tensile pre-strain

In the case of the ST β sample under X-Tensile pre-strain, microstructures in the 2nd and 5th β grains are shown in Fig. 12(a) and (b), respectively. The volume fraction of each variant as a function of time within the two β grains is shown in Fig. 12(c) and (d), respectively. In both β grains, more than 4 different variants are selected. The micro-DVS values in the 2nd and 5th β grains are $R_{VS}^2 = 0.743$ and $R_{VS}^5 = 0.673$, respectively. Different from the previous case presented in Section 3.6.2, the difference of the micro-DVS is relatively small within these two grains. The variation of the local stress state within the two β grains is also calculated and shown in Fig. 12(e) and (f). It can be seen that the local stress states within these two prior β grains are also non-uniform, but both of them are under tension only. According to the interaction energy analysis as presented in Fig. 12(g) and (h), within the two β grain variants V3–V6 and V9–V12 are favored by the initial external loading. Again, not all favored variants have been selected during the phase field simulations. Also note that the most pre-

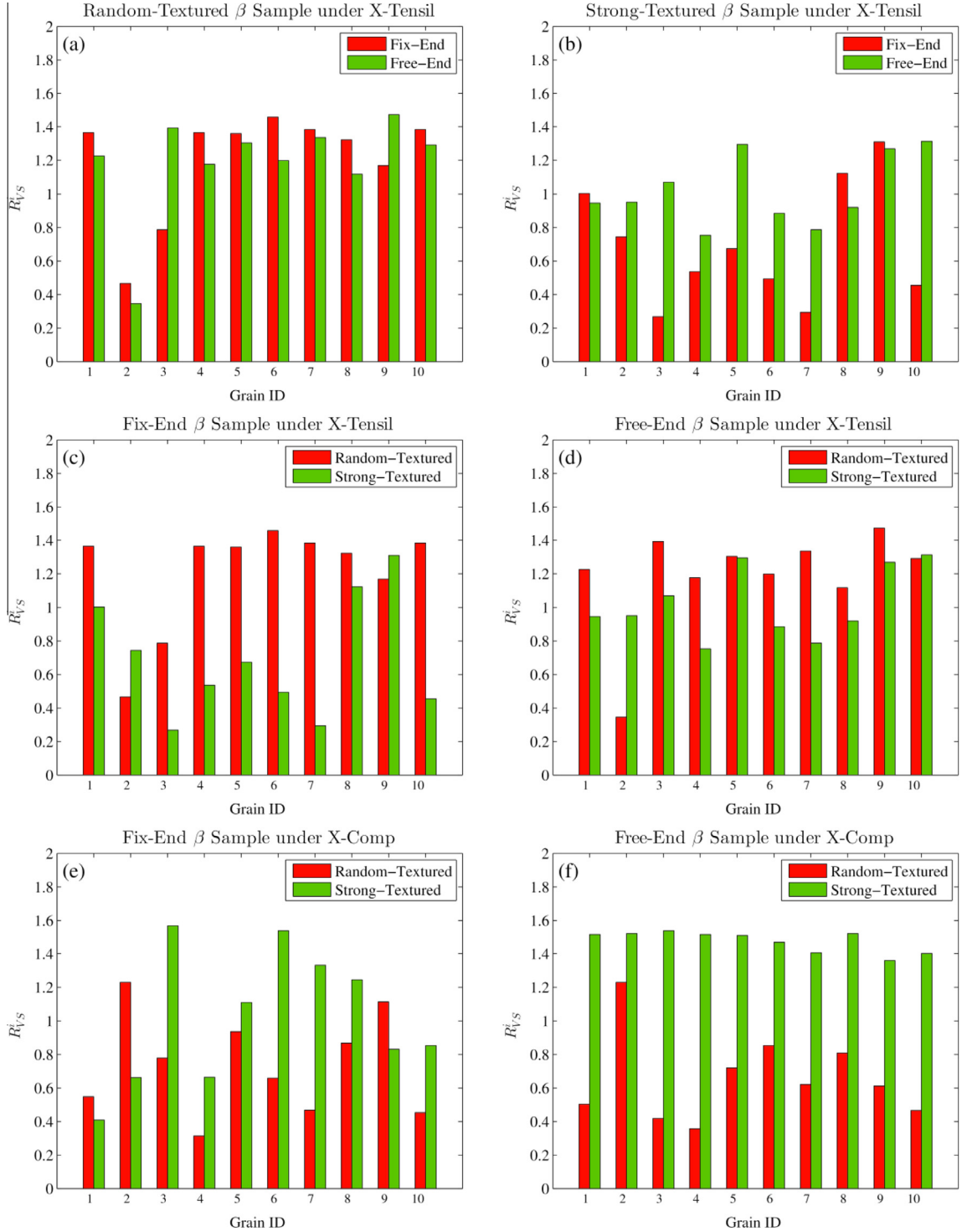


Fig. 10. Responses of micro-DVS, R_{VS}^i , to different processing conditions.

ferred variants by the pre-strain according to the interaction energy calculations do not have the largest volume fractions in the phase field simulations, see, e.g., variant 12 in the 2nd β grain and variant 3 in the 5th β grain. Thus, as compared with the RT sample, there could be a relatively uniform stress state in the ST sample when subjected to a specific pre-strain and such a stress state could promote more α variants simultaneously within the β grains that all have similar orientations.

4. Discussions

4.1. Effect of different processing parameters on variant selection and the resulting transformation texture

A variety of processing parameters could alter the spatial variation of stress/strain fields within the sample during thermo-mechanical processing of titanium alloys. Understanding the influence of these processing parameters on

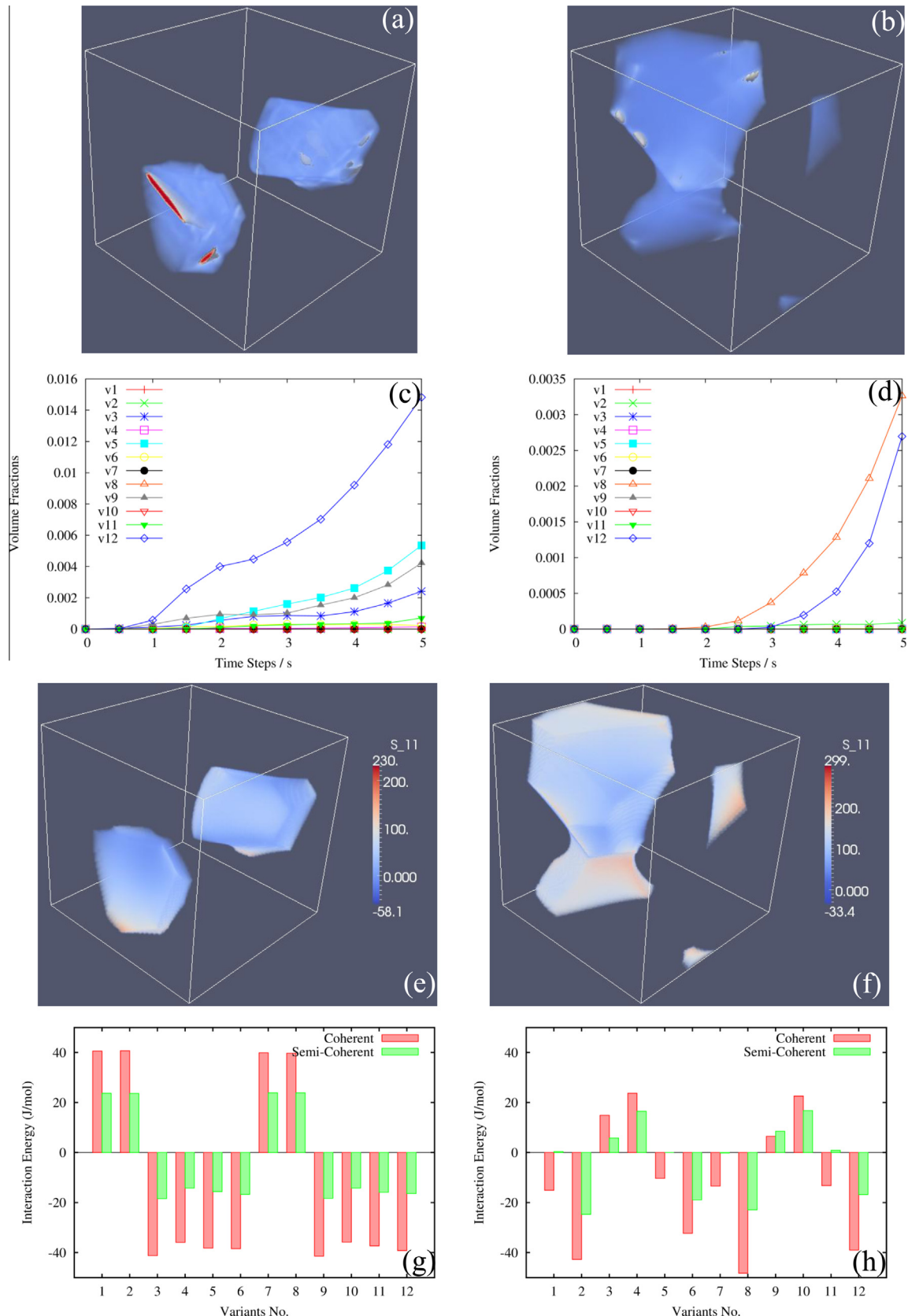


Fig. 11. (a)–(b) $\alpha + \beta$ microstructure in the 2nd and 5th prior β grains in the RT β sample under X -Tensile pre-strain, respectively; (c)–(d) volume fraction of each variant as a function of time; (e)–(f) local stress distribution of σ_{11} ; (g)–(h) interaction energy density between the external loading and each α variant under both coherent and semi-coherent conditions within the two prior β grains.

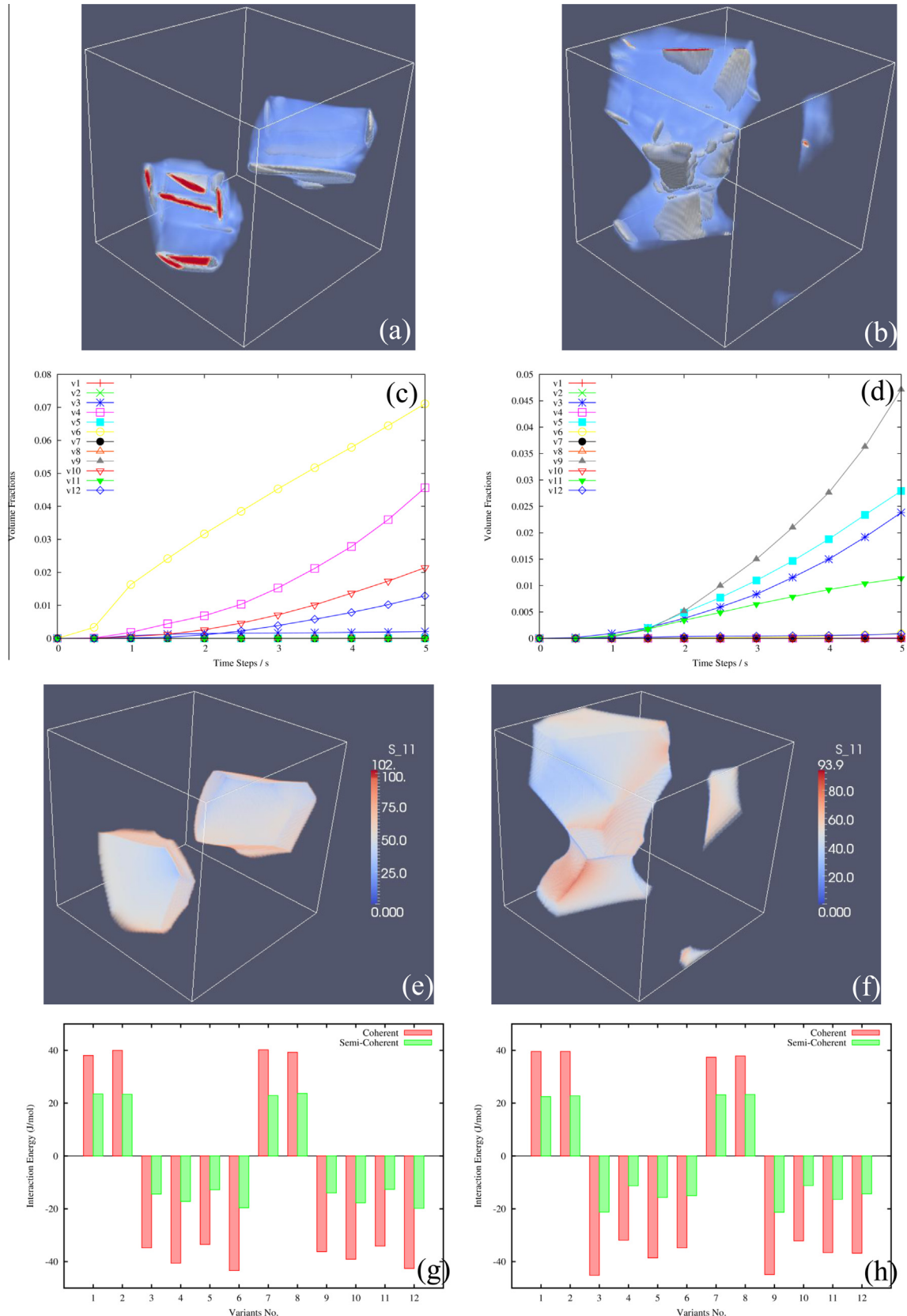


Fig. 12. (a)–(b) $\alpha + \beta$ microstructure in the 2nd and 5th prior β grains in the ST β sample under X -Tensile pre-strain, respectively; (c)–(d) volume fraction of each variant as a function of time; (e)–(f) local stress state σ_{11} ; (g)–(h) interaction energy density between the external loading and each α variant under both coherent and semi-coherent conditions within the two prior β grains.

variant selection (VS) during the $\beta \rightarrow \alpha$ transformation and, in turn, the effect of VS on the strength of transformation texture of the α phase is the major goal of the current study. It is found that both macro-DVS and micro-DVS are significantly smaller in samples without applied pre-strain or stress than those in samples subjected to pre-strain or stress, irrespective of the strength of the starting β phase texture. Local stresses arising from elastic inhomogeneity of a polycrystalline volume element subjected to strain or stress (thermal or applied) are responsible for the variant selection. The degree of variant selection in both the individual β grain and the polycrystalline volume element levels are sensitive to the loading condition, as summarized in Fig. 9(a) and (b). Existing models, which do not account for such a significant variation of local stress and its evolution with microstructure development, may not be able to capture the variant selection and its influence on the transformation texture.

The Fix-End boundary constraint (BC) is more beneficial than the Free-End BC in preventing the development of strong transformation texture for both the ST and RT samples, as shown in Fig. 8(a) and (b). The same conclusion was reached in our recent study on variant selection within a single β grain [12]. The experimental results reported in a recent study on effects of different processing parameters on transformation texture development (due to VS) in Ti-64 sheets during β -processing by Semiatin et al. [64] also support this simulation finding. This phenomenon can be understood by the interplay between the internal stresses created by the pre-strain under the Fix-End BC and the internal stresses associated with an evolving $\alpha + \beta$ microstructure on the development of transformation texture. The latter prefers self-accommodation by autocatalysis and is capable of preventing further development of a strong transformation texture favored by a specific pre-strain. For example even though the Z-Tensile stress preferentially favors a two-variant configuration having a common $(0001)_z$ plane in most of the β grains [12], simulation results show that the ST sample with Fix-End BC still ends up with the smallest macro-DVS and micro-DVS. As shown in Fig. 9(b), F_{VS} are 1.90 and 5.58 in the ST sample under Z-Tensile pre-strain (Fix-End BC) and Z-Tensile external loading (Free-End BC, referred to as Z-Tensile-Free), respectively. If the transformation strain or internal stress produced by α variants selected by a specific pre-strain during early stages of precipitation cannot be accommodated among themselves, the internal stress would prevent further development of such a transformation texture by inducing the formation of other variants to achieve self-accommodation. In addition, the internal stresses associated with α precipitation may also play a role even when a specific pre-strain is able to induce multiple self-accommodating α variants. In the ST sample, for instance, both macro-DVS and micro-DVS are smaller in the case of X-Tensile pre-strain (where more than 5 variants are induced) than those in the case of X-Tensile external stress (see X-Tensile-Free in Fig. 9(b)).

For the sample subjected to the Fix-End BC, F_{VS} are much smaller in the ST sample under different types of pre-strains, excluding the case of X-Comp where F_{VS} are comparable between the RT and ST samples. Zooming into individual β grains in the X-Tensile case, it is also found that the micro-DVS, R_{VS}^i , in most of β grain is much smaller in the ST samples, resulting in a much smaller macro-DVS,

F_{VS} (Fig. 10(c)). According to the interaction energy calculations as shown in Fig. 12(g) and (h) for the ST sample, the initial loading should favor 8 variants in most of the β grains. Such a relatively small degree of variant selection is able to accommodate the transformation strain among the favored variants without resulting in a significant internal stress and the sample ends up with a weak α texture ($F = 24.96$ m.r.d.²). In the RT sample, some β grains may orient to have a relatively large number of α variants favored (e.g., the 2nd grain, $R_{VS}^2 = 0.5577$ while others may only have a limited number of variants preferred by the initial loading (see the red bars in Fig. 10(c)). As a result, both the cumulative VS behaviors in all individual β grains, $\sum_i R_{VS}^i \times V_i$, and the macro-DVS, F_{VS} , are larger in the RT sample as compared with the ST sample (see Fig. 9(a) and (b)). Another possible reason could be the relatively small number of grains in the periodically repeated computational cell.

For β samples subjected to the Free-End BC, F_{VS} is not always smaller in the ST sample (see Fig. 8(b)). For example, F_{VS} is larger ($F_{VS} = 5.618$) in the ST sample in the case of X-Comp external loading. The initial external X-Comp stress favors two pairs of two variants having a common $(0001)_z$ plane in most of the β grains in the ST sample [12]. The development of such a strong texture under the Free-End BC is because of the fact that the transformation strain can be accommodated by the macroscopic shape change of the sample. Moreover, if each β grain contains the same α variants [66], the transformation-induced strains [46] among neighboring grains will be relatively small as well because of the small misorientation among the β grains in the ST sample. As a result, R_{VS}^i is about 1.5 (close to 1.692) in most of the β grains (see the green bars in Fig. 10(f)). In contrast, in the RT sample under the same external X-Comp stress, R_{VS}^i is much smaller, with the largest $R_{VS}^2 = 1.231$ and the smallest $R_{VS}^4 = 0.357$, which also leads to a relatively small $F_{VS} = 3.295$. In the RT sample, on one hand, some β grains are oriented to have a relatively large number of α variants preferred simultaneously by the specific loading. On the other hand, even though some other β grains may have only a limited number of α variants favored by the loading (e.g. the 2nd β grain where 2 pairs of α variants having a common $(0001)_z$ plane are favored by the initial loading), a strong micro-texture may not be able to develop completely. This is because, firstly, the RT sample with strong VS within individual β grains will result in a relatively large transformation-induced strain between adjacent grains. The relaxation of the strain energy will lead to the formation of multi-variants. Secondly, the stress distribution within individual β grains in the RT sample is less uniform than that in the ST sample, which in general favors more α variants. Therefore, the RT sample is not as sensitive to boundary constraints as the ST sample is, as demonstrated in Fig. 9(a) and (b).

4.2. Limited power of variant selection prediction by interaction energy calculations

It has been shown [12,26] that the elastic interaction energy calculation, under the assumption of uniform stress (Sachs assumption) in the entire sample, fails to explain variant selection behavior. As has been pointed out earlier that, within an isolated β grain, the interaction energy

calculations, though simple and analytical, cannot predict the overall VS behavior in all cases and the prediction is valid only when the internal stress generated by the evolving microstructure is significantly smaller than the externally applied stress. The failure of VS prediction by the interaction energy calculation in a β grain embedded in a polycrystalline sample may be attributed to multiple reasons:

- (1) The stress distribution within a polycrystalline β sample subjected to either an applied stress or pre-strain is highly non-uniform and varies significantly from grain to grain, see, e.g., Fig. 11(e) and (f). Furthermore, the stress field keeps evolving during α precipitation.
- (2) The presence of grain boundaries in polycrystalline β samples may affect the VS process. For example, favored α variants with their habit planes parallel to grain boundary planes (GBP) should be able to enjoy extended growth along the GBP. Apparently, such an influence depends on grain size and grain geometry.
- (3) There exists elastic coupling among prior β grains, which makes α precipitation in different grains dependent on each other and, thus, different from that in a single crystal (isolated grain).

4.3. Different measures to quantify macro-degree of variant selection

According to Semiatin et al. [64], macro-DVS could also be quantified using the ratio, R_{VS} , of the maxima pole intensities in the $\{0001\}_\alpha$ and $\{011\}_\beta$ pole figures. For instance, the macro-texture of the RT sample is represented using three different pole figures, $\{101\}_\beta$, $\{111\}_\beta$ and $\{112\}_\beta$ poles, which are the three components in characterizing the BOR, as shown in Fig. 13(a). The corresponding macro-texture of the final α phase without the occurrence of VS is represented using the three corresponding pole figures of the α phase according to the BOR, i.e. $\{0001\}_\alpha$, $\{2\bar{1}\bar{1}0\}_\alpha$ and $\{01\bar{1}0\}_\alpha$. It can be readily seen that, provided no VS, the corresponding $\{101\}_\beta$ and $\{0001\}_\alpha$ pole figures will be identical (see comparison between Fig. 13(a) and (b)), and thus $R_{VS} \equiv 1$. It has been thus concluded that [64] when there is no VS, $R_{VS} \equiv 1$ and whenever VS occurs, $R_{VS} > 1$. It is then believed that the larger the R_{VS} is, the larger the overall degree of VS will be. However, there is a special case where even VS already occurs, one still has $R_{VS} \equiv 1$. For example, another set of ODF for the final α texture from the RT sample is obtained by assuming a special VS occurring in only one β grain where orientation density of the β grain is inherited by all 12 α variants in such a way that multiple random distributions of six α variants are 3 times those of the other 6 α variants sharing a common $\{0001\}_\alpha$ pole. In other words, in the given β grain, VS results from the bias between any two variants with misorientation of $10.5^\circ/[0001]_\alpha$. While in all the other β grains, their orientation density is still shared equally by all 12 α variants within them. The resulting macro-texture of the final α phase is represented using three different pole figures, $\{0001\}_\alpha$, $\{2\bar{1}\bar{1}0\}_\alpha$, and $\{01\bar{1}0\}_\alpha$ as well. It can be found easily that the $\{110\}_\beta$ poles are still identical to the $\{0001\}_\alpha$ pole though variant selection occurs. The occurrence of variant selection can be noticed by comparing the difference between the $\{2\bar{1}\bar{1}0\}_\alpha$ or

$\{01\bar{1}0\}_\alpha$ poles in cases with and without VS in Fig. 13(b) and (c). Thus, using R_{VS} is not able to evaluate critically the influence of a different set of processing variables on the macro-DVS. As a matter of fact, as a 2-D projection of the 3-D orientation distribution, pole figures will bear some losses in information. Thus, the evaluation of degree of variant selection by comparing two sets of pole figures may be inadequate. Instead, the usage of the texture index F to estimate macro-DVS can avoid such a problem. Texture index is the integration of $f^2(\mathbf{g})$ over the entire $\text{SO}(3)$, while for pole intensity, $f(\mathbf{g})$ is integrated only along a specific path within $\text{SO}(3)$ corresponding to the specific poles. As shown in Fig. 13(d), if no variant selection occurs, one has $R_{VS} = 1$ and $F_{VS} = 1$; however, if a special variant selection as the one described in Fig. 13(c) occurs, one has $R_{VS} = 1$ and $F_{VS} = 1.13$. Thus, F_{VS} is a better measure than R_{VS} to quantify macro-DVS.

4.4. Possible two-dimensional sampling effect

The shapes of α precipitates are strongly anisotropic. This anisotropy in shape may lead, even in the absence of variant selection, to a non-uniform variant distribution in a given two-dimensional (2D) cross-section. For example, as shown in Fig. 14, three different cross-sections have been made perpendicular to the x , y and z axes. Obviously the α precipitate microstructures look significantly different at these three cross-sections, as shown by inverse pole figures in Fig. 14(a)–(c). Variant selection is then studied, from a statistical point of view, using the average texture obtained by a virtual EBSD scan through these cross-sections. Apparently, the final α phase texture varies significantly from one cross-section to another in terms of the maximum pole intensity and intensity distribution within each basal pole figure (Fig. 14(a')–(c')). This is due purely to the 2D sampling artifact that has recently been referred to as “pseudo variant selection” [25]. Thus, when analyzing experimental data in the literature one has to bear in mind this possible 2D sampling effect.

4.5. Limitations and future extensions of the model

The current work focuses on VS results from local stresses arising from elastic inhomogeneity of a polycrystalline volume element subjected to an external strain or stress (thermal or applied). In most cases, however, nucleation and growth of α phase may start from prior β grain boundaries (GBs). When the cooling rate is relatively low or the aging temperature is relative high, VS of GB α by prior β grain boundaries and its effect on subsequent intra-granular α precipitate microstructure development needs to be considered. VS of GB α arises from differences in orientation relationships of GB α with respect to both adjacent β grains and in habit plane orientations of GB α relative to the grain boundary inclination among all 12 candidate GB α variants. Some empirical rules have been proposed to explain the effect of these grain boundary parameters on VS of GB α [55,67–69]. Nevertheless, not a single rule or even a combination of different rules is general, i.e., they are not always followed and could all be violated [24,67]. Until now, except on specific special β grain boundaries [55], it is not feasible to make satisfactory prediction toward VS of GB α on a general GB and its effect on both microstructure and transformation texture

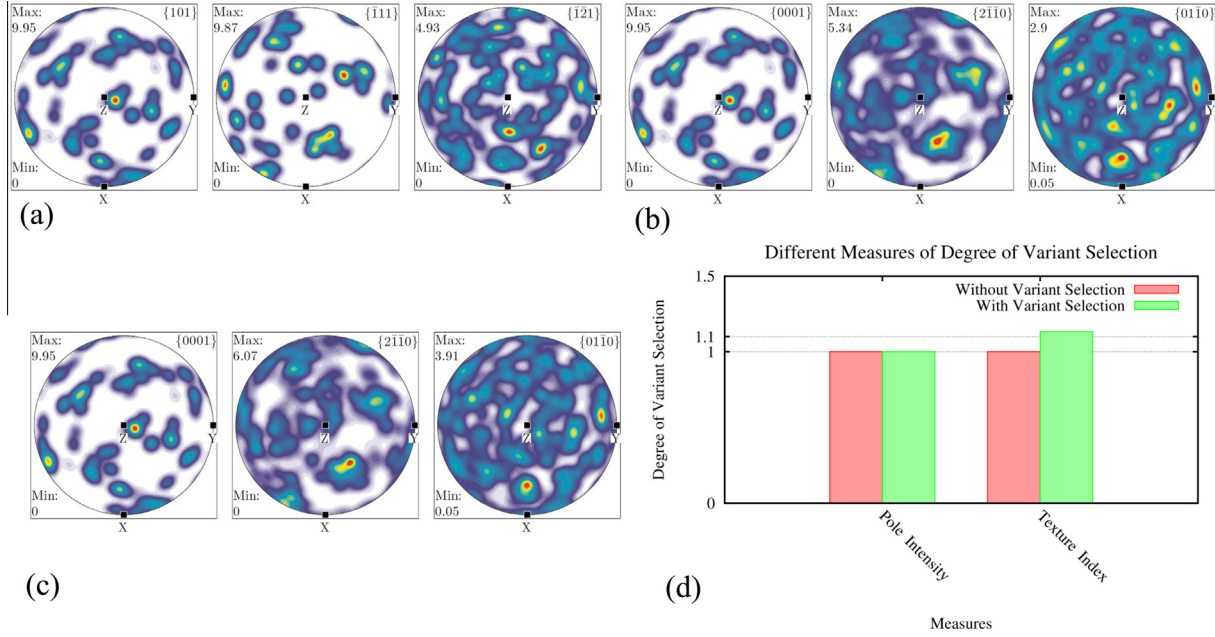


Fig. 13. (a) Macro-texture of the random-textured β sample represented by three different pole figures, $\{101\}_\beta$, $\{111\}_\beta$ and $\{112\}_\beta$ poles, respectively; (b) macro-texture of α phase without the occurrence of variant selection represented by the corresponding three different pole figures, $\{0001\}_\alpha$, $\{2\bar{1}\bar{1}0\}_\alpha$, and $\{01\bar{1}0\}_\alpha$, respectively; (c) macro-texture of α phase with the occurrence of a special variant selection represented by corresponding three different pole figures, $\{0001\}_\alpha$, $\{2\bar{1}\bar{1}0\}_\alpha$, and $\{01\bar{1}0\}_\alpha$, respectively; (d) degrees of variant selection quantified by pole intensity and texture index.

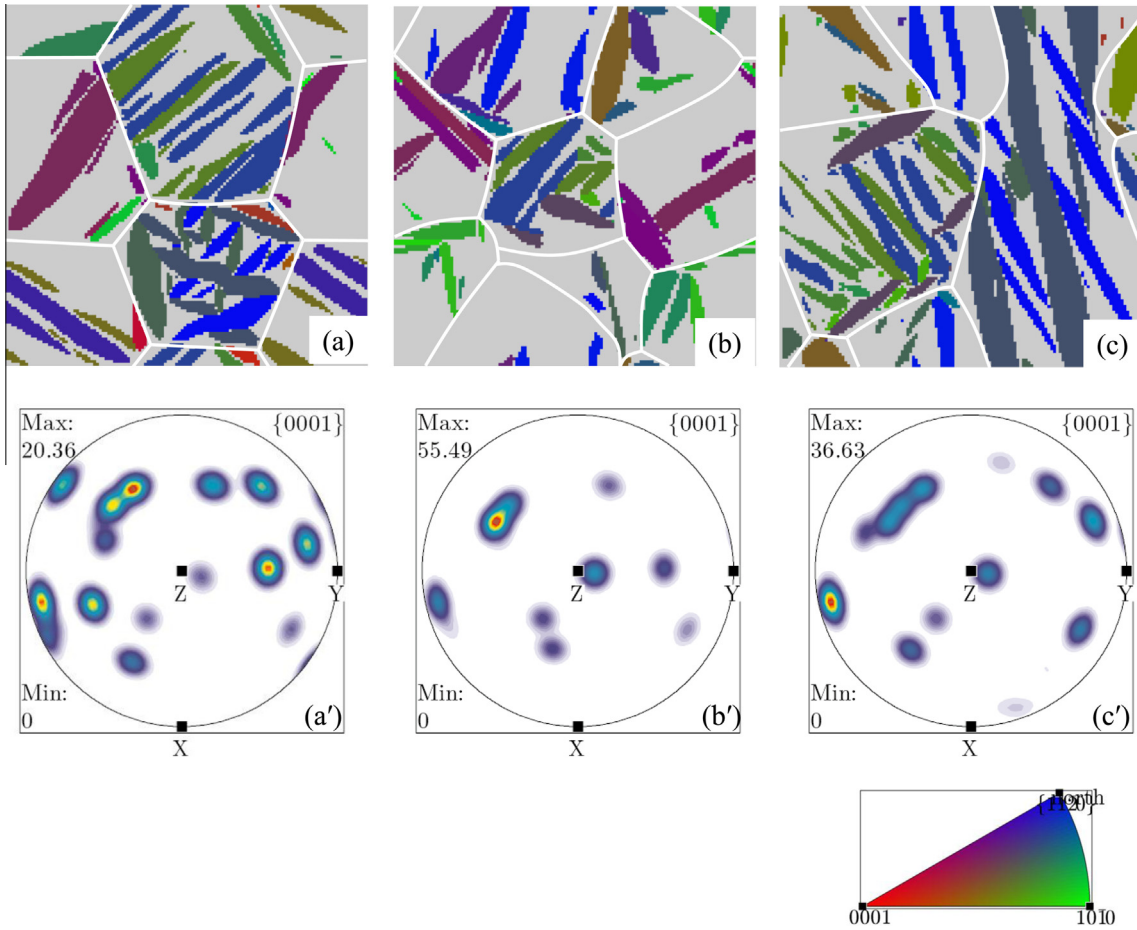


Fig. 14. Examples showing the *pseudo* variant selection due to 2D sampling effect. (a)–(c) Inverse pole figures of different 2D cross-sections; (a')–(c') pole figures corresponding to three different EBSD scans performed at different 2D cross-sections of the 3D volume element.

evolution in β grains. A systematic study of VS by grain boundaries and its interplay with VS by elastic inhomogeneity as a function of aging temperature or cooling rate will be investigated in a separate paper.

It is assumed that there is no misfit strain relaxation at the grain boundaries. The degree of the misfit strain relaxation at the grain boundaries has been found to have a strong influence on the nucleation and growth of the α phase near grain boundaries [70]. However, there is no finding yet that different variants may have different amounts of relaxation at a given grain boundary, similar influence should exist for all 12 α variants and thus would not contribute to VS.

5. Summary

Variant selection (VS) during $\beta \rightarrow \alpha$ transformation in polycrystalline β volume elements under different processing conditions is investigated quantitatively via computer simulations using a three-dimensional phase field model. To mimic sampling material from different locations in a titanium alloy component (which may have experienced different thermal mechanical processing history, or have different boundary constraints, and thus may have different initial β phase texture and different internal stress/strain states), simulation volume elements with differing pre-strains, applied stresses, boundary constraints and starting textures of the β grains are considered. In particular, the effects of VS on both $\alpha + \beta$ microstructure evolution and transformation texture development are captured simultaneously via orientation distribution function (ODF) modeling of the $\alpha + \beta$ two-phase microstructure obtained from the phase field simulations. The variant selection behaviors at both the individual β grain and the overall polycrystalline volume element levels are examined and the α phase texture is found to be sensitive to all the processing variables considered. In particular, VS is found to be most strongly influenced by the local stresses arising from the elastic inhomogeneity of a polycrystalline β volume element subjected to a pre-strain or an applied stress and their interactions with the local stress field associated with α precipitation. The major findings are as follows:

- (1) When subjected to a certain pre-strain, the polycrystalline β volume elements with strong starting textures induce the formation of more α variants simultaneously in all β grains and thus lead to a relatively weaker transformation textures.
- (2) The Fix-End (clamped) boundary condition is more beneficial as compared to the Free-End (relaxed) boundary condition in preventing the formation of strong transformation texture because competition between the internal stress associated with an evolving $\alpha + \beta$ microstructure and the pre-strain would promote the formation of other variants to achieve self-accommodation that is not allowed by strong α texture.
- (3) Variant selection in a polycrystalline volume element having a strong starting texture of the β grains is more sensitive to the boundary constraint than that in volume elements with a weaker starting texture.

These findings may shed light on how to control processing conditions to reduce the strength of transformation texture at both the individual β grain and the overall

polycrystalline volume element levels according to its starting β texture.

To the best of our knowledge, this study represents the first integration of phase field simulations with orientation distribution function modeling to investigate simultaneously microstructure and transformation texture evolutions in polycrystalline volume elements. The method developed will most likely find more applications in investigating transformation texture development during solid-solid transformation in other systems where the product and parent phases exhibit a specific orientation relationship such as in steels, zirconium-alloys and shape memory alloys.

Acknowledgments

We thank Prof. Dipankar Banerjee at the Indian Institute of Science for many valuable discussions. This work is supported by the NSF DMREF program under Grant No. DMR-1435483 and US DARPA under Contract HR0011-12-C-0035.

References

- [1] H. Bhadeshia, R. Honeycombe, Steels: Microstructure and Properties: Microstructure and Properties, Butterworth-Heinemann, 2011.
- [2] J.-F. Nie, 20 – Physical metallurgy of light alloys, in: D.E.L. Hono (Ed.), Physical Metallurgy, fifth ed., Elsevier, Oxford, 2014, p. 2009.
- [3] J. Mohd Jani, M. Leary, A. Subi, M.A. Gibson, A review of shape memory alloy research, applications and opportunities, Mater. Des. 56 (2014) 1078.
- [4] G. Kurdjumov, G. Sachs, Z. Phys. 64 (1930) 225.
- [5] Z. Nishiyama, Sci. Rep. Res. Inst. Tohoku Univ. 23 (1934) 638.
- [6] G. Wassermann, Arch. Eisenhuttenwes 16 (1933) 647.
- [7] E.C. Bain, Trans. AIME 70 (1924) 25.
- [8] W.G. Burgers, On the process of transition of the cubic-body-centered modification into the hexagonal-close-packed modification of zirconium, Physica 1 (1934) 561.
- [9] W. Pitsch, A. Schrader, Arch. Eisenhutten Wes. 29 (1958) 715.
- [10] D. Banerjee, J.C. Williams, Perspectives on titanium science and technology, Acta Mater. 61 (2013) 844.
- [11] G. Lutjering, J.C. Williams, Titanium (Engineering Materials and Processes), Springer, Berlin, 2007.
- [12] R. Shi, Y. Wang, Variant selection during α precipitation in Ti-6Al-4V under the influence of local stress – a simulation study, Acta Mater. 61 (2013) 6006.
- [13] R. Whittaker, K. Fox, A. Walker, Texture variations in titanium alloys for aeroengine applications, Mater. Sci. Technol. London 26 (2010) 676.
- [14] G.A. Sargent, K.T. Kinsel, A.L. Pilchak, A.A. Salem, S.L. Semiatin, Variant selection during cooling after beta annealing of Ti-6Al-4V ingot material, Metall. Mater. Trans. A 43A (2012) 3570.
- [15] R.A. Winholtz, Residual stresses: macro and micro stresses, in: K.H.J. Buschow, W.C. Robert, C.F. Merton, I. Bernard, J.K. Edward, M. Subhash, V. Patrick (Eds.), Encyclopedia of Materials: Science and Technology, Elsevier, Oxford, 2001, p. 8148.
- [16] L. Zeng, T.R. Bieler, Effects of working, heat treatment, and aging on microstructural evolution and crystallographic texture of $[\alpha]$, $[\alpha']$, $[\alpha'']$ and $[\beta]$ phases in Ti-6Al-4V wire, Mater. Sci. Eng. A 392 (2005) 403.
- [17] M. Humbert, L. Germain, N. Gey, P. Bocher, M. Jahazi, Study of the variant selection in sharp textured regions of bimodal IMI 834 billet, Mater. Sci. Eng. A 430 (2006) 157.
- [18] H. Moustahfid, M. Humbert, M.J. Philippe, Modeling of the texture transformation in a Ti-64 sheet after hot compression, Acta Mater. 45 (1997) 3785.

- [19] N. Gey, M. Humbert, M.J. Philippe, Y. Combres, Modeling the transformation texture of Ti-64 sheets after rolling in the [beta]-field, *Mater Sci Eng. A* 230 (1997) 68.
- [20] N. Gey, M. Humbert, M.J. Philippe, Y. Combres, Investigation of the alpha- and beta-texture evolution of hot rolled Ti-64 products, *Mater. Sci. Eng. a – Struct.* 219 (1996) 80.
- [21] D. Qiu, R. Shi, D. Zhang, W. Lu, Y. Wang, Variant selection by dislocations during α precipitation in α/β titanium alloys, *Acta Mater.* 88 (2015) 218.
- [22] S. Kar, R. Banerjee, E. Lee, H.L. Fraser, Influence of crystallography variant selection on microstructure evolution in titanium alloys, in: J.M. Howe, D.E. Laughlin, J.K. Lee, U. Dahmen, W.A. Soffa (Eds.), *Solid–Solid Phase Transformation in Inorganic Materials*, vol. 1, TMS, 2005.
- [23] E. Lee, R. Banerjee, S. Kar, D. Bhattacharyya, H.L. Fraser, Selection of alpha variants during microstructural evolution in alpha/beta titanium alloy, *Philos. Mag.* 87 (2007) 3615.
- [24] S.M.C. van Bohemen, A. Kamp, R.H. Petrov, L.A.I. Kestens, J. Sietsma, Nucleation and variant selection of secondary alpha plates in a beta Ti alloy, *Acta Mater.* 56 (2008) 5907.
- [25] A.F. Gourgues-Lorenzon, Application of electron backscatter diffraction to the study of phase transformations, *Int. Mater. Rev.* 52 (2007) 65.
- [26] M. Humbert, B. Gardiola, C. Esling, G. Flemming, K.E. Hensger, Modelling of the variant selection mechanism in the phase transformation of HSLA steel produced by compact strip production, *Acta Mater.* 50 (2002) 1741.
- [27] P.S. Bate, W.B. Hutchinson, Imposed stress and variant selection: the role of symmetry and initial texture, *J. Appl. Crystallogr.* 41 (2008) 210.
- [28] M. Ueda, H.Y. Yasuda, Y. Umakoshi, Effect of grain boundary character on the martensitic transformation in Fe-32at.%Ni bicrystals, *Acta Mater.* 49 (2001) 3421.
- [29] R. Shi, N. Ma, Y. Wang, Predicting equilibrium shape of precipitates as function of coherency state, *Acta Mater.* 60 (2012) 4172.
- [30] J.W. Cahn, J.E. Hilliard, Free energy of a nonuniform system. I. Interfacial free energy, *J. Chem. Phys.* 28 (1958) 258.
- [31] L.D. Landau, E. Lifshitz, On the theory of the dispersion of magnetic permeability in ferromagnetic bodies, *Phys. Z. Sowjetunion* 8 (1935) 101.
- [32] J.S. Rowlinson, The thermodynamik theory of capillarity under the hypothesis of a continuous variation of density (Translation of J.D. van der Waals'), *J. Stat. Phys.* 20 (1979) 197.
- [33] J.D. Eshelby, The determination of the elastic field of an ellipsoidal inclusion, and related problems, *Proc. R. Soc. London Ser. A* 241 (1957) 376.
- [34] J.D. Eshelby, The elastic field outside an ellipsoidal inclusion, *Proc. R. Soc. A* 252 (1959) 561.
- [35] A. Khachaturyan, Some questions concerning the theory of phase transformations in solids, *Sov. Phys. Solid State* 8 (1967) 2163.
- [36] A.G. Khachaturyan, *Theory of Structural Transformations in Solids*, John Wiley & Sons, New York, 1983.
- [37] A.G. Khachaturyan, G.A. Shatalov, Elastic interaction potential of defects in a crystal, *Sov. Phys. Solid State* 11 (1969) 118.
- [38] W.J. Boettinger, J.A. Warren, C. Beckermann, A. Karma, Phase-field simulation of solidification, *Annu. Rev. Mater. Res.* 32 (2002) 163.
- [39] L.-Q. Chen, Phase-field models for microstructure evolution, *Annu. Rev. Mater. Res.* 32 (2002) 113.
- [40] H. Emmerich, *The Diffuse Interface Approach in Materials Science: Thermodynamic Concepts and Applications of Phase-Field Models*, Springer, 2003.
- [41] Karma A. Phase, Field. Methods, in: K.H.J. Buschow, R.W. Cahn, M.C. Flemings, B. Ilschner, E.J. Kramer, S. Mahajan, P. Veyssiére (Eds.), *Encyclopedia of Materials: Science and Technology*, second ed., Elsevier, Oxford, 2001, p. 6873.
- [42] C. Shen, Y. Wang, Coherent precipitation - phase field method, in: S. Yip (Ed.), *Handbook of Materials Modeling. Models*, vol. B, Springer, New York, 2005, p. 2117.
- [43] Y. Wang, L.Q. Chen, N. Zhou, *Simulating Microstructural Evolution using the Phase Field Method. Characterization of Materials*, John Wiley & Sons Inc, 2012.
- [44] Y.U. Wang, Y.M. Jin, A.G. Khachaturyan, Dislocation Dynamics—Phase Field, *Handbook of Materials Modeling*, Springer, 2005, p. 2287.
- [45] H.J. Bunge, *Texture Analysis in Materials Science – Mathematical Methods*, London, 1982.
- [46] A. Artemev, Y.M. Jin, A.G. Khachaturyan, Three-dimensional phase field model and simulation of cubic \rightarrow tetragonal martensitic transformation in polycrystals, *Philos. Mag. A* 82 (2002) 1249.
- [47] I. Steinbach, F. Pezzolla, B. Nestler, M. Seebelberg, R. Prieler, G.J. Schmitz, J.L.L. Rezende, A phase field concept for multiphase systems, *Phys. D* 94 (1996) 135.
- [48] I. Steinbach, F. Pezzolla, A generalized field method for multiphase transformations using interface fields, *Phys. D* 134 (1999) 385.
- [49] Y.U. Wang, Y.M.M. Jin, A.G. Khachaturyan, Phase field microelasticity theory and modeling of elastically and structurally inhomogeneous solid, *J. Appl. Phys.* 92 (2002) 1351.
- [50] Y.U. Wang, Y.M. Jin, A.G. Khachaturyan, Three-dimensional phase field microelasticity theory of a complex elastically inhomogeneous solid, *Appl. Phys. Lett.* 80 (2002) 4513.
- [51] Y.U. Wang, Y.M.M. Jin, A.G. Khachaturyan, Mesoscale modelling of mobile crystal defects – dislocations, cracks and surface roughening: phase field microelasticity approach, *Philos. Mag.* 85 (2005) 261.
- [52] Y. Shen, Y. Li, Z. Li, H. Wan, P. Nie, An improvement on the three-dimensional phase-field microelasticity theory for elastically and structurally inhomogeneous solids, *Scr. Mater.* 60 (2009) 901.
- [53] O. Engler, V. Randle, *Introduction to Texture Analysis: Macrotecture, Microtexture, and Orientation Mapping*, CRC Press, 2009.
- [54] F. Bachmann, R. Hielscher, H. Schaeben, Texture analysis with MTEX-free and open source software toolbox, *Solid State Phenom.* 160 (2010) 63.
- [55] R. Shi, V. Dixit, H.L. Fraser, Y. Wang, Variant selection of grain boundary α by special prior β grain boundaries in titanium alloys, *Acta Mater.* 75 (2014) 156.
- [56] G.C. Obasi, R.J. Moat, D.G. Leo Prakash, W. Kockelmann, J. Quinta da Fonseca, M. Preuss, In situ neutron diffraction study of texture evolution and variant selection during the alpha to beta to alpha phase transformation in Ti-6Al-4V, *Acta Mater.* 60 (2012) 7169.
- [57] G.C. Obasi, S. Biroscă, D.G.L. Prakash, J.Q. da Fonseca, M. Preuss, The influence of rolling temperature on texture evolution and variant selection during alpha \rightarrow beta \rightarrow alpha phase transformation in Ti-6Al-4V, *Acta Mater.* 60 (2012) 6013.
- [58] N. Stanford, P.S. Bate, The martensitic transformation texture in Ti-6Al-4V, in: *ICOTOM 14: Textures of Materials*, Pts 1 and 2, vol. 495–497, 2005, p. 669.
- [59] S.C. Wang, M. Aindow, M.J. Starink, Effect of self-accommodation on alpha/alpha boundary populations in pure titanium, *Acta Mater.* 51 (2003) 2485.
- [60] D. Banerjee, Private communication, 2014.
- [61] C.H. Rycroft, VORO plus plus: a three-dimensional Voronoi cell library in C plus, *Chaos* 19 (2009) 04111.
- [62] J. Gruber, N. Ma, Y. Wang, A.D. Rollett, G.S. Rohrer, Sparse data structure and algorithm for the phase field method, *Modell. Simul. Mater. Sci. Eng.* 14 (2006) 1189.

- [63] R. Shi, Y. Wang, Variant selection during alpha precipitation in titanium alloys: A simulation study, in: ProQuest Dissertations and Theses, The Ohio State University, 2014, ISBN 9781321477146, p. 399 (in English) <http://search.proquest.com/docview/1647259296?accountid=9783>.
- [64] S.L. Semiatin, K.T. Kinsel, A.L. Pilchak, G.A. Sargent, Effect of process variables on transformation-texture development in Ti-6Al-4V sheet following beta heat treatment, *Metall. Mater. Trans. A* 44 (2013) 3852.
- [65] D.Y. Li, L.Q. Chen, Selective variant growth of coherent Ti₁₁Ni₁₄ precipitate in a TiNi alloy under applied stresses, *Acta Mater.* 45 (1997) 471.
- [66] Y. Gao, R. Shi, J.F. Nie, S.A. Dregia, Y. Wang, Deformation path degeneracy in structural transformations, Unpublished work.
- [67] T. Furuhara, S. Takagi, H. Watanabe, T. Maki, Crystallography of grain boundary α precipitates in a β titanium alloy, *Metall. Mater. Trans. A* 27 (1996) 1635.
- [68] N. Stanford, P.S. Bate, Crystallographic variant selection in Ti-6Al-4V, *Acta Mater.* 52 (2004) 5215.
- [69] M. Salib, J. Teixeira, L. Germain, E. Lamielle, N. Gey, E. Aeby-Gautier, Influence of transformation temperature on microtexture formation associated with alpha precipitation at beta grain boundaries in a beta metastable titanium alloy, *Acta Mater.* 61 (2013) 3758.
- [70] T.W. Heo, L.-Q. Chen, Phase-field modeling of displacive phase transformations in elastically anisotropic and inhomogeneous polycrystals, *Acta Mater.* 76 (2014) 68.